

五百米口径球面射电望远镜脉冲星研讨会(2)

Invited speakers

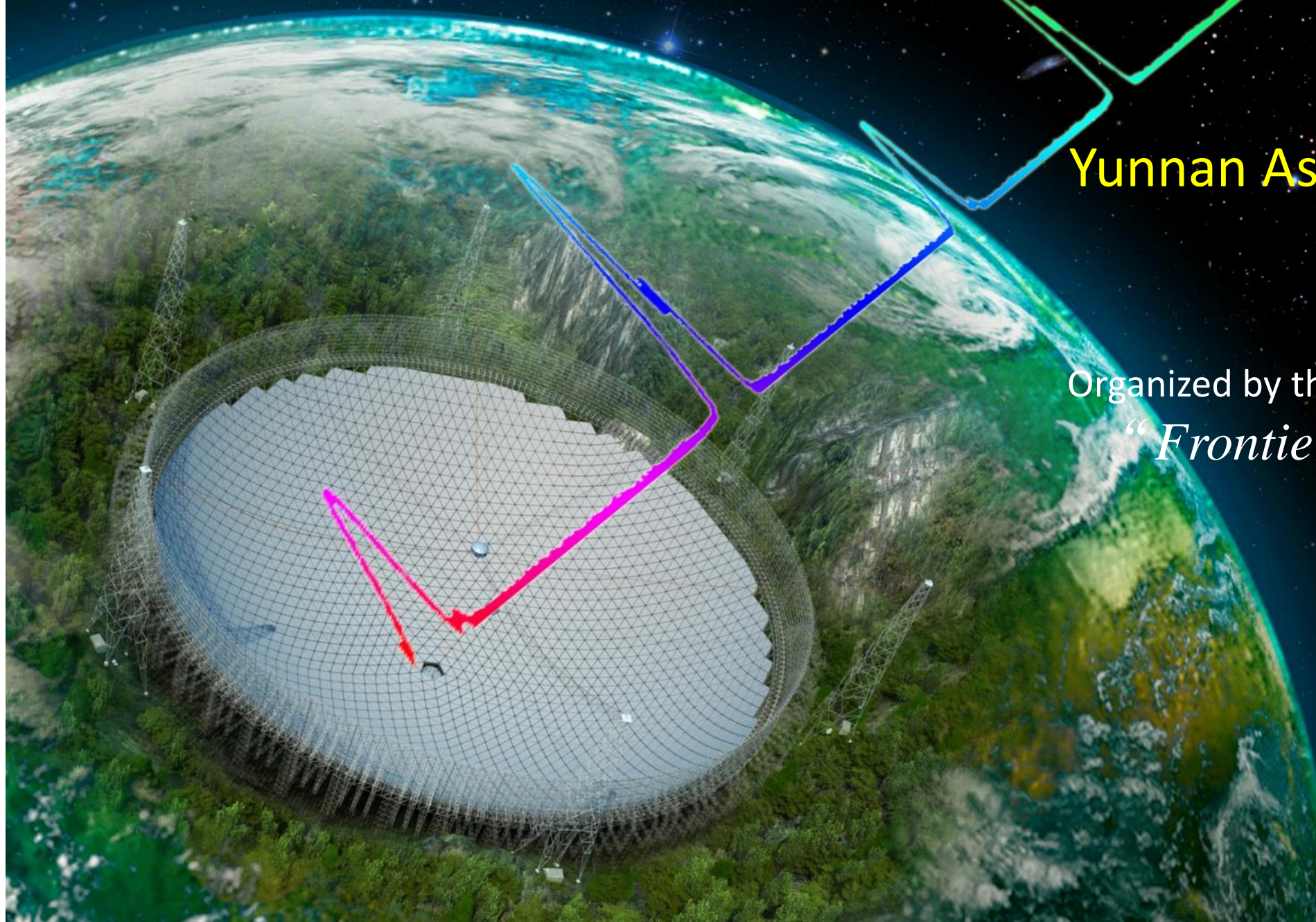
Fredrick Jenet (UTB)
Andrew Siemion (UC Berkeley)

Local organizers

Min Wang (YNAO)
Longfei Hao (YNAO)
Zhixuan Li (YNAO)
Yonghua Xu (YNAO)
Jiang Dong (YNAO)

FAST Pulsar Symposium 2

<http://fps2013.csp.escience.cn>



Yunnan Astronomical Observatory
Kunming, Yunnan
July 1-3, 2013

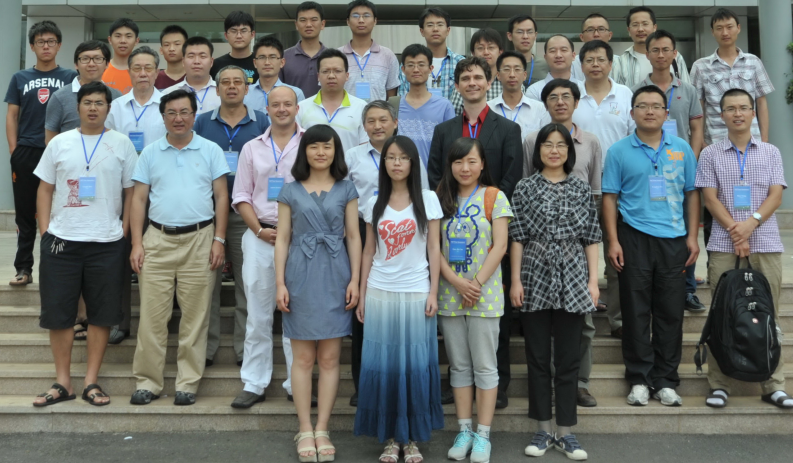
Organized by the pulsar group of the '973' project

*“Frontiers in Radio Astronomy and
FAST Early Science”*

Di Li (NAOC)
Renxin Xu (PKU)
Jianping Yuan (XAO)
Yefei Yuan (USTC)
Youling Yue (NAOC)
Chengmin Zhang (NAOC)

第二届 500 米口径球面射电望远镜脉冲星项目组讨论会

FAST Pulsar Symposium II



500 米口径球面射电望远镜脉冲星组专题研讨会

第二次会议

位于我国贵州的 500 米口径球面射电望远镜 (Five hundred meters Aperture Spherical Telescope, 简称 FAST) 正在建设之中, 其建成将是世界上最大的单口径射电望远镜。脉冲星研究是 FAST 的重要科学内容, 也为国家重点基础研究发展计划 (即“973 计划”) 之一——“射电波段前沿天体物理课题及 FAST 早期科学的研究”的课题 1 所关注。脉冲星研究人才的培养迫在眉睫; 此 FPS 系列会议的宗旨就是为了有效地推动国内脉冲星研究学者之间的交流、了解国际研究进展、培育未来射电脉冲星骨干, 见证中国脉冲星研究队伍的成长、壮大历程。

作为“973 计划”项目的一部分, 脉冲星组 (“课题 1”) 组织的每年一次 FPS 会议以中国脉冲星学者为主, 并邀请部分国际同行参加。第一次会议于 2012 年 8 月 13 日至 16 日在新疆昌吉园林宾馆举行。这次是第二次会议, 于 2013 年 7 月 1 日至 3 日在云南昆明滇池宾馆召开。

脉冲星是高速自转的强磁场天体, 对脉冲星的研究可以促进关于致密物态、引力与相对论、星系天文学、天体测量学、行星物理甚至宇宙学等方面的认识。除了这些科学意义外, 脉冲星研究还具有时间标准和导航等工程学应用价值。包括地面 FAST 和空间 HXMT 等大科学工程的实施预示着中国脉冲星研究美好的未来。让我们期待我国学者在国际脉冲星研究舞台上辉煌的表现!

科学组委会:
973 计划脉冲星组

地方组委会:
云南天文台 汪敏, 郝龙飞, 李志玄, 徐永华, 董江

贰零壹叁年玖月

目 录

1. The effect of differential rotation on the evolution of spin rate and temperature of accreting millisecond neutron stars	曹国洁	1
2. 用微引力透镜方法测量孤立中子星的质量	代实	4
3. Constraining Braking Indexes of Magnetars by Their Associated Supernova Remnants	高志福	7
4. 磁星的 X 射线能谱	郭彦君	11
5. XTE J1701-462 水平分支准周期震荡	李兆升	14
6. kHz QPO models confront correlations between kHz and LF QPOs in NS XBs	李志兵	17
7. Energy dependence of LF QPOs for BH H1743-322 and NS Cyg X-2	李志兵	20
8. 振荡驱动的脉冲星辐射	林梦翔	21
9. 回落盘的制动：从射电脉冲星到磁星	刘雄伟	23
10. 通过 X 射线偏振辨别脉冲星结构模型	卢吉光	26
11. How to check the pulsar radio radiation models observationally?	乔国俊	28
12. SGR 短爆能量来源	屈稚杰	31
13. 磁星辐射机制研究	全号	33

14. kHz QPO 对中子星的质量半径估计	王德华等.....	34
15. Understanding Isolated And Accreting Magnetars In Hard X-rays	王伟.....	37
16. 对称能：从两味到三味？	徐仁新.....	46
17. 上海 65 米射电望远镜脉冲星观测研究	阎振等.....	48
18. Re-processing the Parkes Multi-beam Pulsar Survey Data: Software test and initial result	于萌	51
19. Magnetar Giant Flares and Precursors	余聰	54
20. 脉冲星的到达时间观测	袁建平等.....	57
21. 40 米望远镜脉冲星搜索终端	岳友岭，朱岩.....	60
22. 脉冲星周期跃变中的能量释放	周恩平.....	62
23. 会议日程.....		64

The effect of differential rotation on the evolution of spin rate and temperature of accreting millisecond neutron stars

Guo-Jie Cao

Xinjiang Astronomical Observatory

CAS

Urumqi 830011

P. R. China

Email: caoguojie@xao.ac.cn

1 Introduction

Neutron stars are cosmic laboratories of nature of the materials that under extreme conditions. The physics of the inner regions of the neutron stars are still not perfectly coherent. Fortunately, we can learn this region by investigate the thermal and spin evolution of the neutron stars [1] [2].

R-modes are quasi-toroidal oscillations in rotating stars that the Coriolis force acts as the restoring force. In [3], the authors modeled the interactions between r-modes together with basic neutron star physics including spin and thermal evolution of the star. This provide us a new way to investigate the thermal evolution of the neutron stars which make it possible to investigate making use of the observational data. So far, r-mode in neutron stars was extensively studied in accreting systems (e.g. [4, 5]).

Cuofano [6] found that in the previous models the only damping mechanism for the r-mode instability that against the driven effect gravitational radiation is too simple, and it can not explain the phenomenology of the millisecond pulsars in LMXBs which rotate at frequency above 200 Hz. So the authors introduced the magnetic damping rate for the first time in the r-modes equations. But they did not take into account the second order effect, mainly the differential rotation, which induced by the r-modes and can not be ignored [7].

In this paper, we investigated through the r-modes the evolution of the magnetic field and the thermal evolution of accreting millisecond neutron stars in Low Mass X-ray Binaries (LMXBs) taking into account both the magnetic damping rate and the second order effect. So we would find that the spin and thermal evolution of the neutron stars are remarkably influenced by the differential rotation.

2 R-mode equations

First of all, we model the r-mode equations. We start by considering the conservation of angular momentum. The r-mode is driven by the gravitational waves and damped by the viscosity [3] as well as the generated toroidal magnetic field [8]. The angular momentum of the star is affected by gravitational waves, accreting matters and the dipole field. Get these issues together, we get the r-mode equations :

$$\frac{d\alpha}{dt} = \alpha[F_g - (F_v + F_{mi})] + \frac{1}{3}\alpha^3 Q[4(K+2)F_g - (4K+5)(F_v + F_{mi})] - \frac{\alpha\dot{M}}{2\tilde{I}\Omega}(\frac{G}{MR^3})^{1/2} + \frac{\alpha F_{me}}{2}, \quad (1)$$

$$\frac{d\Omega}{dt} = -\frac{2}{3}\alpha^2\Omega Q[4(K+2)F_g - (4K+5)(F_v + F_{mi})] + \frac{\dot{M}}{\tilde{I}}(\frac{G}{MR^3})^{1/2} - \Omega F_{me} - \Omega\frac{\dot{M}}{M}. \quad (2)$$

where α is the r-mode's amplitude, F_g , F_v , F_s are gravitational radiation growth rate, shear viscous damping rate, bulk viscous damping rate, respectively. $Q=3\tilde{J}/(2\tilde{I})=0.094$.

Notice that F_{mi} is the magnetic damping rate, and in our model, it is modified because of the second-order effect,

$$F_{mi}(t) = \frac{dE_M^N/dt}{E_r} \simeq \frac{8(1-p)}{9\pi p(4K+9)\tilde{J}} \frac{B_d^2 R \Lambda' \int_0^t \alpha^2(t') \Omega(t') dt'}{M\Omega} \quad (3)$$

where E_M^N is the magnetic energy in the case that the stellar core is composed a normal neutron fluid, $dE_M^N/dt=[\frac{4(1-p)}{9\pi p}]B_d^2 R^3 \Lambda' \alpha^2(t) \Omega(t) \int_0^t \alpha^2(t') \Omega(t') dt'$ [8], $p=0.5$, and $\Lambda' \simeq 1$. The integration time here takes contribution from the phase during which the star is still inside the instability region.

Together with the thermal evolution equation, we solve these equations numerically.

3 Results

Fig 1 and fig 2 are part of the result obtained by solving the r-mode equations. Fig 1 shows the evolution of the spin rate of the neutron star with the effect of differential rotation and magnetic damping rate. K is the initial amount of the differential rotation associated with the r-mode. When taking the differential rotation (e.g. $K=100$) into account, a self spin up with dramatic oscillation was found, comparing with the $K=-2$ case. The evolution of temperature of the neutron star is shown in fig 2. A significant heating effect in the differential rotation case was found. For more details, please see an upcoming paper (Cao2013, in preparation).

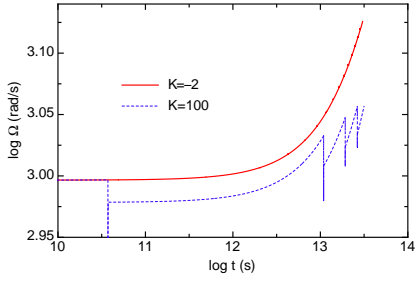


Figure 1: Evolution of the spin rate of the neutron star with the effect of differential rotation and magnetic damping rate. For specific case $K = -2$, there is no differential rotation.

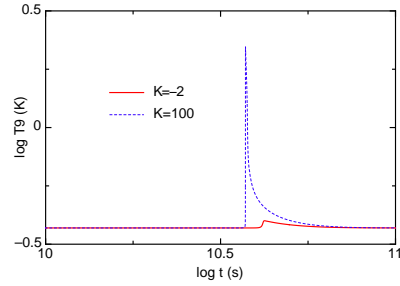


Figure 2: Evolution of the temperature of the neutron star with the effect of differential rotation and magnetic field.

References

- [1] D G Yakovlev, et al., **53**, 1253-1253 (1999)
- [2] D G Yakovlev, K P Levenfish, Yu A Shibanyov, Physics-Uspekhi, **42**, 737 (1999)
- [3] B.J. Owen, L.Lindblom, C.Cutler, B.F. Schutz, A. Vecchio, N. Andersson, Phys. Rev. D, **58**, 084020 (1998)
- [4] N. Andersson, K.D. Kokkotas, N. Stergioulas, ApJ, **516**, 307 (1999)
- [5] Y. Levin, ApJ, **517**, 328 (1999)
- [6] C. Cuofano, A. Drago, Phys. Rev. D, **82**, 084027 (2010)
- [7] P.M. S, Phys. Rev. D, **69**, 084001 (2004)
- [8] L. Rezzolla, Phys. Rev. D, **64** 104014 (2001)

用微引力透镜方法测量孤立中子星的质量

代实 (*Shi Dai*)
北京大学物理学院天文学系
中国 北京 100871
Email: daishi@pku.edu.cn

1 引言

中子星的质量对于我们理解中子星的物态和结构有重要的意义。目前我们对中子星质量的测量主要限制于双星系统中，对于孤立中子星我们仍然没有很好的办法测量质量。在FAST Pulsar Symposium I (FPSI)的会议文集中，我们已经讨论过用微引力透镜效应测量脉冲星质量的可行性。

本文中，我将更新我们得到的最新结果。首先，我将展示中子星对于银河系引力透镜事件的贡献，并且考虑了背景恒星数目随距离变化的影响。然后，我将说明根据我们的计算，通过astrometric microlensing现象，脉冲星的质量能够被较为精确地测定。

2 中子星对银河系引力透镜事件的贡献

引力透镜事件的事件率可以用以下表达式计算，

$$\Gamma = \frac{4G^{1/2}}{c} \int_0^\infty dD_s D_s^{2+2\beta} \rho(D_s) \times \frac{\int_0^{D_s} dD_d \rho(D_d) v [D_d(D_s - D_d)/MD_s]^{1/2}}{\int_0^\infty dD_s D_s^{2+2\beta} \rho(D_s)}, \quad (1)$$

计算中我们使用了最新的孤立脉冲星分布的模拟结果，考虑脉冲星的kick velocity，同时考虑银河系中恒星在盘和核球的空间和速度分布。另外，我们还考虑了由于背景恒星的亮度随距离的增大而降低，以及消光等因素，可观测的背景恒星的数目随距离并不是简单的 $D_d^2 dD_d$ 的关系。我们引进了参数 β 来刻画这些效应， β 的取值在 $-1 \leq \beta \leq -3$ 之间。

用以上模型，我们得到了中子星在不同方向上，对银河系引力透镜事件的贡献，如图1 所示。我们发现中子星主要贡献的是短持续时间的事件，因为中子星有比较大的速度，这与之前没有考虑中子星分布的结果是完全不同的(Wood & Mao 2005, WM05)。另外，我们发现在银盘上，偏离银心的方向上，中子星贡献了绝大部分的短时标时间，这对于我们以后搜寻由中子星导致的引力透镜事件有重要的指导意义。在图表1中，我们列出了对全天平均后得到的中子星对光深和事件率的贡献比例。

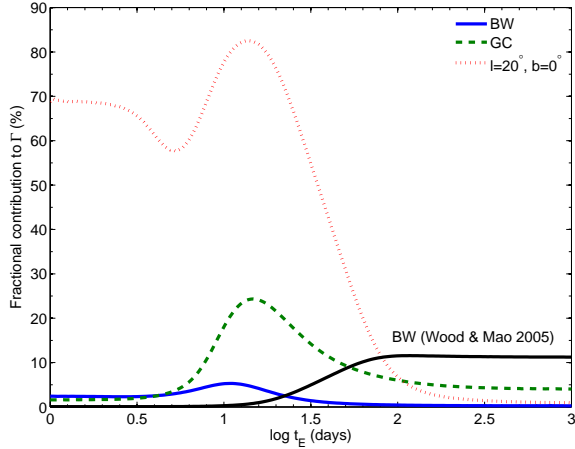


Figure 1: Fractional contributions to the total Galactic event rate, as a function of the event time-scale, from neutron stars. The solid, dashed and dotted lines show the contribution from neutron stars towards the BW, GC and off-GC direction ($l = 20^\circ$, $b = 0^\circ$), respectively. In comparison, the fractional contribution from neutron stars towards the BW based on WM05’s model is shown with dot-dashed line.

Table 1: Percentage contributions to the total predicted τ and Γ , from different types of lens. In comparison, results based on WM05’s model are also shown.

	Models	Types of lens				
		BD	MS	WD	BH	NS
Optical depth	WM05	6.6	62.1	22.2	3.4	5.7
	New NS model	6.4	57.2	20.3	2.8	13.3
Event rate	WM05	17.2	62.1	16.9	0.9	2.9
	New NS model	15.1	54.7	14.9	0.8	14.5

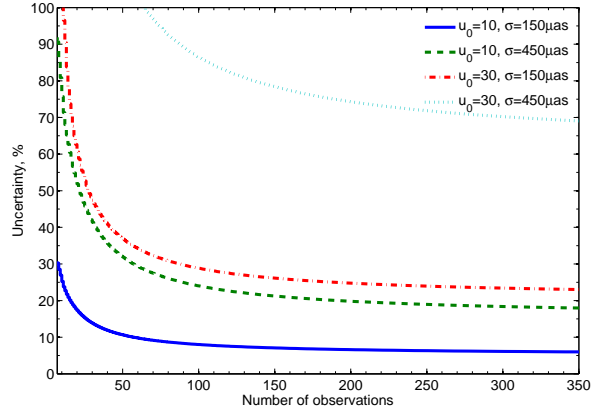


Figure 2: The percentage error in estimation of M as a function of number of data points, for pulsar lenses. We suppose that pulsar distances are tightly constrained through radio observations. Results for different u_0 and σ are shown.

3 质量测量的误差

我们主要考虑了用astrometric microlensing的方法测量脉冲星质量的误差，使用了 covariance analysis 的方法。之所以考虑 astrometric microlensing，是因为这样的事件发生的截面更大，事件率更高，正如我们在之前的文集中讨论的。

图2展示了我们对于脉冲星质量误差估计的结果。对于 $\sigma = 150 \mu\text{as}$ 的光学定位精度， ~ 50 次的观测以及 impact parameter $u_0 = 10$ ，脉冲星的质量能被测量精确到 $\sim 10\%$ 。

4 总结

我们的计算表明，考虑了中子星的分布后，中子星将贡献很高比例的短时标的引力透镜事件。因此未来针对银盘和银心的巡天很有可能发现有中子星和脉冲星导致的事件。我们也展示了，使用引力透镜的方法能较为精确地测量脉冲星的质量。考虑到未来FAST将发现大量的脉冲星，结合未来的光学巡天项目，我们很有希望能用引力透镜的方法测量孤立脉冲星的质量。

References

- [1] Wood A., Mao S. 2005, MNRAS, 362, 945

Constraining Braking Indexes of Magnetars by Their Associated Supernova Remnants

Gao Zhifu

Xinjiang Astronomical Observatory, CAS, 150, Science
1-Street, Urumqi Xinjiang, 830011, P. R. China
Email: zhifu_gao@xao.ac.cn

1 Introduction

As we know, the spin angular frequency ω of pulsars decreases with time, and the time derivative of Ω is proportional to some power of ω ,

$$I\dot{\omega} = -K \omega^n , \quad (1)$$

where $K = 2B^2R^6\sin^2\theta / 3c^2$ is a positive parameter [1]. The braking index n of a pulsar can be measured by differentiating Eq.(1),

$$n = \frac{\ddot{\nu}\nu}{\dot{\nu}^2} , \quad (2)$$

where $\ddot{\nu}$ is the second order time derivative of rotation frequency ν . In the model that assumes spin-down is due to pure magnetodipole radiation with a constant magnetic field, we obtain the ideal values of n in Eqs.(1-2), $n = 3$ [1], [2], [3], [4]. The observed values of n for six radio pulsars always deviate from 3 expected for pure magneto-dipole radiation model.

For magnetars, their extremely strong magnetic fields are at least $10^2 \sim 10^3$ times higher than those of the typical NSs, and as young as young radio pulsars (1-100 kyr). Soft-gamma repeaters(SGRs) or anomalous X-ray pulsars (AXPs) are considered as candidates for magnetars [5], [6]. Up to now, we have detected 23 magnetar candidates (11 SGRs and 12 AXPs), among which three candidates have radio emission. Unfortunately, we can not measure magnetars braking indexes observationally due to strong timing noise and the lack of long-term radio emission.

2 Our methods

In Zhang and Xie (2011) [4], authors suggested that the canonical spin-down age (or canonical characteristic age) of a neutron star(NS) $t_C = P/2\dot{P}$ is not available to

estimate its real age t_R , and the physically meaningful criterion to estimate t_R is the NS-SNR association. Their suggestions are in the same way applicable to magnetars with associated SNRs. From Manchester et al 1985. [7], for a constant braking index n , the characteristic age t is given by

$$t = \frac{\nu}{(1-n)\dot{\nu}}[1 - (\frac{\nu}{\nu_i})^{n-1}] = \frac{P}{(n-1)\dot{P}}[1 - (\frac{P_i}{P})^{n-1}], \quad (3)$$

where ν_i (P_i) is the initial rotation frequency (period). Be note that quite different from the canonical spin-down age t_C , the characteristic age t in Eq.(3) is very close to the real age, t_R , of a NS. For all magnetars with associated SNRs, their values of ν_i are far larger than those of ν , the face rotation frequencies. Thus, the relation of $(\frac{\nu}{\nu_i})^{n-1} = (\frac{P_i}{P})^{n-1} \simeq 0$ is always hold approximately for all magnetar progenitors.

We assume the ages of SNRs to be the real ages of magnetars, and replace a constant braking index with an average braking index,i.e.,

$$t_{\text{SNR}} \sim t_R, \quad n \longrightarrow \tilde{n}. \quad (4)$$

Inserting Eq.(4) into Eq.(3) gives

$$\tilde{n} \approx 1 - \frac{\nu}{\dot{\nu}t_{\text{SNR}}} = 1 + \frac{P}{\dot{P}t_{\text{SNR}}}, \quad (5)$$

where P_i is the initial spin period. Thus, we obtain the average second order time derivative of rotation frequency, $\tilde{\dot{\nu}}$, from

$$\tilde{\dot{\nu}} = \frac{\tilde{n}\dot{\nu}^2}{\nu}. \quad (6)$$

3 Results

Table 1 shows the data on 11 claimed magnetar-supernova remnant associations, which are cited from McGillAXP/SGR online catalog updated except for SGR 1806-20 and SGR 1900+14. Combining Eq.(5-6) with Table 1, we get the values of \tilde{n} and $\tilde{\dot{\nu}}$, as listed in Table 2. For SGR 0501+4516, its value of \tilde{n} is near to the expected value 3, which implies a “quasi” magnetic-dipole braking mechanism. For AXPs 1E 2259+586 and 1E 1841-045, their values of \tilde{n} are larger than 3, whereas for magnetars SGR 0526-66, SGR 1806-20, SGR 1627-41, SGR 1900+14,Swift J1834, 1E 1547.0-5408 and CXOU J1714, their values of \tilde{n} are less than 3.In previous works, many authors proposed various models to explain why the observed braking index $n \neq 3$, eg., neutrino and photon radiation coming from superfluid neutrons, [8],additional torques due to accretion[9], a pulsar wind nebula (PNW) [10], the changes of the

Sources	$P(\text{s})$	$\dot{P}(10^{-11}\text{s s}^{-1})$	$t_C(\text{kyr})$	SNR	$t_{\text{SNR}}(\text{kyr})$
SGR 0526-66	8.0544(2)	3.8(1)	3.4	N49	10 ± 5
SGR 1806-20	7.6022(7)	75(4)	0.16	G10.0-0.3	17 ± 13
SGR 1627-41 ^t	2.594578(6)	1.9(4)	2.2	G33.70-0.1	16.3 ± 13.7
SGR 1900+14	5.19987(7)	9.2(4)	0.90	G42.8+0.6	19.8 ± 10.2
Swift J1834	2.4823018(1)	0.796(12)	1.4	W41	150 ± 50
SGR 0501+4516	5.7620953(3)	0.582(3)	16	HB9	15 ± 3
1E 2259+586	6.9789484460(39)	0.048430(8)	230	CTB109	12 ± 3
1E 1841-045	11.7828977(10)	3.93(1)	4.8	Kes73	1.5 ± 1.0
1E 1547 ^t	2.0721255(1)	4.7	0.70	G327.24-0.13	3.2 ± 1.8
CXOU J1714 [†]	3.82535(5)	6.40(14)	0.95	CTB37B	3.2 ± 1.7
AX J1845 [†]	6.97127(28)	—	—	G29.6+0.1	15.3 ± 14.7

Table 1: Observed parameters of magnetars and their SNRs. All data are from the McGill AXP/SGR online catalog of 1 June 2013 (<http://www.physics.mcgill.ca/pulsar/magnetar/main.html>). The sign ^tdenotes: A transient AXP. The sign [†] denotes: This candidate is unconfirmed.

magnetic field B , the magnetic inclination angle θ , moment of inertia I and magnetospheres conductivity, and so on.

I am grateful to Yunnan Astronomical Observatory, CAS and Peking University for providing this opportunity, and I thank Prof. R.X.Xu and Prof. B.P. Gong for their valuable suggestions which help me to improve this paper substantially.

References

- [1] R. N. Manchester, J. H. Taylor,: Pulsars. San Francisco, CA(USA): W. H. Freeman, 281p (1977).
- [2] R. D. Blandford, R. W. Romani, Mon. Not. R. Astron. Soc. **234**, 57 (1988).
- [3] K. Menou, R. Perna, L. Hernquist, Astrophys. J. Lett. **554**, 63 (2001).
- [4] S. N. Zhang, Y. Xie, ASP Conference Series, Vol. 451. Edited by S. Qain, K. Leung, L. Zhu, and S. Kwok. San Francisco: Astronomical Society of the Pacific, **451**, 231 (2011).
- [5] C. Thompson, R. C. Duncan, Mon. Not. R. Astron. Soc.**275**, 255 (1995).
- [6] C. Thompson, R. C. Duncan, Astrophys. J. **473**, 322 (1996)

Sources	$\dot{\nu}(\text{s}^{-2})$	$\tilde{\nu} (\text{s}^{-3})$	\tilde{n}
SGR 0526–66	$-5.85(15) \times 10^{-13}$	$(5.259 \pm 1.301) \times 10^{-24}$	1.908 ± 0.472
SGR 1806–20	$-1.30(7) \times 10^{-11}$	$(1.3459 \pm 1.2735) \times 10^{-21}$	1.048 ± 0.038
SGR 1627–41	$-3.32(9) \times 10^{-12}$	$(5.3207 \pm 2.0633) \times 10^{-23}$	1.861 ± 0.722
SGR 1900+14	$-3.40(15) \times 10^{-12}$	$(6.7684 \pm 0.4147) \times 10^{-24}$	1.126 ± 0.069
Swift J1834	$-1.29(2) \times 10^{-12}$	$(7.2310 \pm 1.0678) \times 10^{-24}$	1.751 ± 0.258
SGR 0501+4516	$-1.753(9) \times 10^{-13}$	$(5.9321 \pm 1.4027) \times 10^{-25}$	3.354 ± 0.55
1E 1547.0–5408	$-1.0946259(1) \times 10^{-11}$	$(4.0695 \pm 0.8926) \times 10^{-25}$	1.639 ± 0.359
1E 2259+586	$-9.9433(2) \times 10^{-15}$	$(2.6962 \pm 0.526) \times 10^{-26}$	39.082 ± 7.618
1E 1841–045	$-2.830(7) \times 10^{-13}$	$(1.6373 \pm 0.8728) \times 10^{-23}$	17.351 ± 9.249
CXOU J1714	$-4.37(9) \times 10^{-12}$	$(1.4172 \pm 0.8728) \times 10^{-22}$	1.94 ± 0.35

Table 2: Braking indexes and frequency parameters of magnetars.

- [7] R. N. Manchester, et al, Nature. **313**, 374 (1985).
- [8] Q. H. Peng, K. L. Huang, J. H. Huang, Astron. Astrophys. **107**, 258 1982
- [9] W. C. Chen, X. D. Li, Astron. Astrophys. **450**, L1 (2006)
- [10] A. K. Harding, I, Contopoulos, D, Kazanas, Astrophys. J. Lett. **525**, 125 (2001).

Discussion

Prof. B.P. Gong (Hua-Zhong science and technology University.): You can firstly estimate the ratios of $n\dot{u}/\dot{\nu}$ and $n\ddot{u}/\dot{\nu}$ for different magnetars, then discuss their braking indexes.

Dr. Z.F. Gao(Xinjiang Astronomical Observatory, CAS.): I will do as your suggestions. Thank you very much.

磁星的X射线能谱

郭彦君 (Yanjun Guo)
北京大学物理学院
天文系
中国 北京 100871
Email: guoyj10@pku.edu.cn

1 引言

反常X射线脉冲星(Anomalous X-ray Pulsars, AXPs)和软 γ 射线重复爆 (Soft Gamma-ray Repeaters, SGRs)是一类特殊的脉冲星类天体。其中AXPs是作为软X射线源被发现的；它的X射线光度大于自转能损（不是转动供能），同时又没有伴星存在的迹象（不是吸积供能）。AXPs的能源机制成谜，由此得名反常X射线脉冲星。SGRs是通过硬X射线/软 γ 射线波段的短爆发探测到的，最初被认为是 γ 射线爆；但它的特征光子能量低一些，并且有重复爆发现象，所以归类为软 γ 射线 重复爆。然而，AXPs和SGRs并没有本质区别；一些AXPs也探测到了短爆，而处于宁静态的SGRs与 AXPs表现相似。现在一般认为AXPs和SGRs是同一类脉冲星类天体，它们的特殊表现对传统的中子星模型 提出了重大挑战。

在AXPs/SGRs的研究中，能量来源是一个基本问题。磁星模型认为AXPs/SGRs具有超强磁场，由磁场衰减供能。其他解释需要借助于来自超新星回落盘的吸积。确定AXPs/SGRs是磁星还是回落盘系统有重要意义，它不仅有助于解释高能天体物理现象，也可以帮助我们理解致密物质的物态。近年来，多波段观测揭示了AXPs/SGRs的更多奇异之处，对上述理论模型作出了限制。这里主要讨论硬X射线辐射。

软X射线成分在AXPs发现之时就已探测到，可以用黑体谱加软幂率谱来拟合。近来，在一些AXPs/SGRs中观测到了硬X射线辐射，能谱性质与软X射线波段有很大差异。硬X射线能谱一般可以用较硬的幂率谱拟合，并且能量与软X射线波段相当。目前有一些试图解释硬X射线辐射物理机制的想法。在磁星框架下，Baring 和 Harding提出表面光子与磁层电子的共振逆康普顿散射 (Resonant Inverse Compton Scattering, RICS) 过程可以产生延伸到MeV的 幂率谱，谱指数约为1 [1]。回落盘框架下，Trümper et al.考虑了由种子光子在吸积流中的整体运动康普顿散射(bulk-motion Comptonization, BMC)过程来解释硬X射线辐射 [2]。他们的工作表明，对于4U 0142+61 (最亮的AXP，并且在红外波段观测到了回落盘迹象)， BMC模型可以同时拟合软X射线和硬X射线能谱。

2 X射线能谱

限制硬X射线辐射的不同模型可以帮助我们理解AXPs/SGRs的本质，这也是我们工作的动机所在。如前文所述，BMC模型在解释0142的能谱时很成功，但它还有待进一步检验。BMC模型能否应用于其他AXPs/SGRs？或者说，吸积图像是否能普遍地解释AXPs/SGRs的X射线辐射？Suzaku对一些AXPs/SGRs的观测首次提供了同时观测的软硬X射线数据 [3]。我们从中选取了4颗较为明亮的源，提取了它们的能谱并尝试用BMC模型拟合。

另一个问题是，如何区分不同的模型，比如RICS和BMC？受限于硬X射线望远镜的灵敏度和观测时间，目前的数据还不足以达成此目标。但未来硬X射线调制望远镜(HXMT)——中国第一颗天文卫星——也许会改变这种情况。HXMT接收面积大，因而具有高灵敏度。基于Trümper et al.的参数，之前对于0142的HXMT模拟显示，RICS与BMC模型之间存在分歧；鉴于RICS是延伸到MeV的幂率谱，而BMC则可能在几百 keV处出现截断。所以我们也用HXMT的响应矩阵模拟了20-250 keV的BMC能谱，如果在此能段出现截断，那么可以期待通过未来HXMT的观测区分RICS与BMC模型。

能谱拟合时，BMC过程由Xspec中的模型comptb描述，考虑了种子光子的BMC与TC效应。根据我们的结果，BMC模型可以很好地拟合这四颗源的能谱，但对参数的限制较差。每颗源都可以得到几组不同的参数，问题主要在于 δ （BMC与TC的效率之比）和 kT_e （电子温度）的简并，这是Suzaku数据在硬X射线波段的低信噪比导致的。对于这些不同的参数，HXMT的模拟结果也不同。一般地， kT_e 越低，截断出现越早。

我们试图从物理上对参数加以限制，但并未得到结果。INTEGRAL具有比Suzaku更高的能段，所以我们想借助INTEGRAL的观测来限制参数。为了得到可以接受的信噪比，我们把迄今所有的公开数据加在一起，总观测时间~ 10 Ms。

对于INTEGRAL的数据，用BMC拟合时可以得到一组 $\chi^2/d.o.f.$ 明显更好的参数。图1给出了AXP 1RXS J1708-40的能谱，可以看到~ 100 keV处的截断；其他源的情况类似。

3 结论

AXPs/SGRs是磁星还是回落盘系统？我们试图从硬X射线辐射方面来理解这一问题。所选4颗源的能谱都可以很好地用BMC拟合，这暗示着吸积流的存在，是对回落盘模型的支持。而且在HXMT的能量范围内，能谱很可能出现截断。未来HXMT的观测有望区分RICS和BMC模型，进而帮助我们理解AXPs/SGRs的本质。

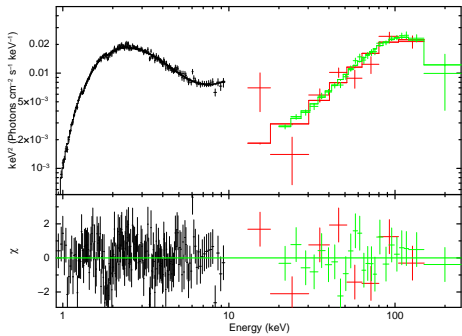


Figure 1: 1RXS J1708-40的能谱, Suzaku, INTEGRAL数据和HXMT模拟分别用黑色, 红色, 绿色表示。

References

- [1] M. G. Baring, A. K. Harding, Ap&SS, **308**, 109 (2007)
- [2] J. E. Trümper, A. Zezas, Ü. Ertan et al., A&A, **518**, A46 (2010)
- [3] T. Enoto, K. Nakazawa, K. Makishima et al., ApJ, **722**, L162 (2010)

XTE J1701-462 水平分支准周期震荡

李兆升
北京大学物理学院
天文系
中国 北京 100871
Email: lizhaosheng@pku.edu.cn

1 引言

准周期震荡现象在 X 射线双星系统中普遍存在。按频率大小，准周期震荡可分为低频准周期震荡 (Low-frequency QPO, 100 Hz 以下) 和千赫兹准周期震荡 ($10^2 - 10^3$ Hz)。千赫兹 QPO 一般成对出现，间隔 200 – 400 Hz，在黑洞暂现源和中子星双星中都能观测到，这种 QPO 可能来自于致密星吸积伴星物质的开普勒运动。在中子星双星中，Z 源低频准周期震荡可按分支不同，分为水平分支准周期震荡 (HBO)、正常分支准周期震荡 (NBO) 和耀发分支准周期震荡 (FBO)。黑洞暂现源中，可分为 A 型、B 型和 C 型 QPO。Casella 等人[1]认为 Z 源的 HBO、NBO 和 FBO 分别对应于黑洞暂现源中的 C 型、B 型和 A 型 QPO。Z 源的 HBO 和黑洞暂现源的 C 型 QPO 可能和吸积盘的进动有关，也即 Lense-Thirring 效应，Lense-Thirring 进动的频率为[2]:

$$\nu_{LT} = \frac{G Ma}{\pi c^2 r^3} = \frac{8\pi^2 I \nu_K^2 \nu_s}{c^2 M} = 13.2 I_{45} \left(\frac{M}{M_\odot} \right)^{-1} \left(\frac{\nu_K}{1000 \text{Hz}} \right)^2 \left(\frac{\nu_s}{300 \text{Hz}} \right) \text{Hz}, \quad (1)$$

其中， M 为致密星质量， a 为角动量， $I = 10^{45} I_{45}$ g cm² 为转动惯量， ν_s 为自转频率， ν_K 为开普勒频率。这个模型解释了 Atoll 源 4U 1728-34、4U 0614+091 和 KS 1731-260 的低频 QPO。但是，最近发现了自转频率为 11 Hz 的毫秒脉冲星 IGR J17480-2446[3]，其低频 QPO 在 35-50 Hz 之间，千赫兹的 QPO 在 800-920 Hz 之间，由中子星的状态方程， $I_{45}/(M/M_\odot) < 2$ ， $\nu_{LT} < 0.82$ Hz，远远小于观测到的低频 QPO 频率，这给 Lense-Thirring 进动模型带来了挑战。本文研究了 XTE J1701-462 的 HBO 现象，验证 HBO 与盘的内半径是否满足 Lense-Thirring 模型的预计，并讨论 HBO 可能的起源。

2 观测

在 2006-2007 年间，RXTE 卫星对 XTE J1701-462 做了 866 次观测，总时长约为 3 Ms。XTE J1701-462 在爆发过程中，经历了 Cyg-like Z 源、Sco-like Z 源

和 Atoll 源阶段。这是到目前为止，唯一的一个观测到在这三种态之间演化的中子星低质量X射线双星源。

我们用 Heasoft 6.12 软件包，从 *RXTE* 卫星的 PCU2 标准 2 模式的数据中，抽取绝对能道分别为 6-9, 10-17, 18-23 和 24-43 的光变曲线，时间分辨率为 16 s，并扣除背景。我们定义 Soft Color 为 10-17 ($\sim 4.5\text{-}7.4 \text{ keV}$) 能道与 6-9 ($\sim 2.9\text{-}4.1 \text{ keV}$) 能道的计数率之比，Hard Color 为 24-43 ($\sim 10.2\text{-}18.1 \text{ keV}$) 能道与 18-23 ($\sim 7.8\text{-}9.8 \text{ keV}$) 能道的计数率之比，强度为 $\sim 2.9\text{-}18.1 \text{ keV}$ 能段的计数率。我们选择了 XTE J1701-462 处在典型的 Cyg-like 和 Sco-like 阶段时的数据，color-color diagram (CCD) 见图 1。

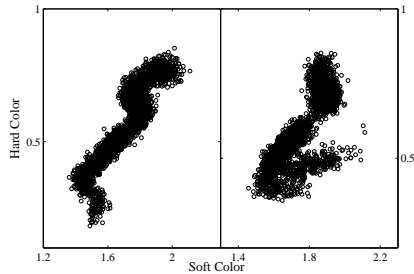


Figure 1: Cyg-like 态和 Sco-like 态的 CCD.

用带吸收的多温盘、黑体、铁线、截断幂律模型拟合 XTE J1701-462 的能谱，可以从中获取其内盘半径。结合水平分支 QPO 的中心频率，可以验证 XTE J1701-462 的内盘半径和中心频率之间的关系是否满足 Lense-Thirring 模型的预言。结果如图 2 所示。无论 XTE J1701-462 处于 Cyg-like 阶段还是 Sco-like 阶段，内盘半径和 HBO 的中心频率都是正相关，与 Lense-Thirring 模型的预言不符。

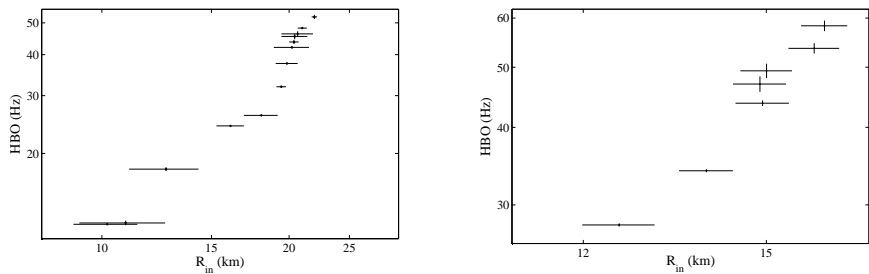


Figure 2: Cyg-like 态和 Sco-like 态的内盘半径与HBO的中心频率的关系.

3 讨论

Lense-Thirring 吸积盘进动模型常被用来解释中子星双星的低频 QPO 以及黑洞双星的 C 型 QPO。但是，此模型认为吸积盘的内半径和HBO的中心频率 ν 应满足 $\nu \propto r_{\text{in}}^{-3}$ 。我们拟合 XTE J1701-462 的能谱时发现，吸积盘的内半径和 HBO 正相关，这表明，XTE J1701-462的 HBO 并不是来自于吸积盘的进动，有可能形成于双星冕区的非热辐射，这种QPO的形成机制在Yan[4]等人的工作中也有讨论。

References

- [1] P. Casella, T. Belloni and L. Stella, **ApJ**, 629,403 (2005)
- [2] L. Stella, M. Vietri et al., **ApJ**,524, L63 (1999)
- [3] D. Altamirano, et al., **ApJ**,759, L20 (2012)
- [4] S.P. Yan, N. Wang, G.Q. Ding, and J.L. Qu, **arXiv:1303.0085**, (2013).

kHz QPO models confront correlations between kHz and LF QPOs in NS XBs

Li Zhibing

Xinjiang Astronomical Observatory, Chinese Academy of Sciences, 150, Science 1-Street, Urumqi, Xinjiang 830011, China
 Email: lizhibing@xao.ac.cn

1 Observations

The kHz QPO was firstly detected in Sco X-1 by RXTE van der Klis et al. 1996. Up to now, 34 NS LMXBs are reported to exhibit kHz QPOs. We have collected all the available informations of the kHz QPOs of these sources from the published papers. Among these sources, however, only 24 of the 34 sources have simultaneous frequency measurements of the kHz and LF QPOs. For those 24 sources, the frequency correlations between the kHz and LF QPOs are shown in Fig. 1.

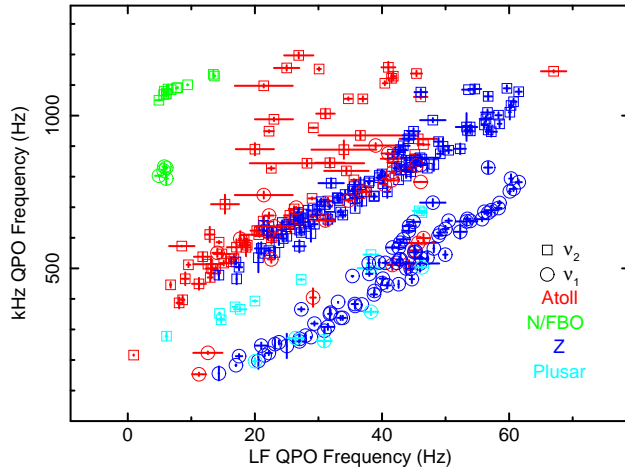


Figure 1: Frequency correlations between kHz and LF QPOs. The open squares and circles stand for the lower and upper kHz QPOs, respectively. The red, blue and light blue points denote the kHz and LF QPO correlations of atoll, Z and millisecond plusar respectively. The green points represent the frequency correlations between kHz QPOs and possible NBOs/FBOs.

2 Theoretical Models

We use the following models to fit the data of Cyg X–2, GX 5–11, GX 17+2 and GX 340+0.

2.1 General relativity precession model

In the general relativity precession model, the theoretical relations between the frequencies of kHz and LF QPOs as follows (Stella & Vietri 1998):

$$\nu_{lf} \simeq 297.3\phi^{-5/2}m^{2/3}\left(\frac{\nu_2}{1000}\right)^{5/3}[1 + 0.15\phi^{-1}\left(\frac{m\nu_2}{1000}\right)^{2/3}]. \quad (1)$$

$$\nu_{lf} \simeq 500\phi^{-5/2}\left(\frac{\nu_1}{500}\right)[1 - 0.19(1 - \phi^{-1})\left(\frac{m\nu_1}{500}\right)^{2/5}], \quad (2)$$

As shown by Equations 1 and 2, the correlations between kHz and LF QPOs in the general relativity precession model depend on the two parameters, i.e., m and ϕ .

2.2 Alfvén wave oscillation model

During the Alfvén wave oscillation model (Zhang 2004), the correlations between frequencies of the kHz and LF QPOs are

$$\nu_{lf} \simeq 386A^{-1}\phi^{-3}\left(\frac{\nu_2}{1000}\right)^2[1 + 0.08A^{-2/3}\phi^{-1}\left(\frac{\nu_2}{1000}\right)^{2/3}], \quad (3)$$

$$\nu_{lf} \simeq 500\phi^{-3}\left(\frac{\nu_1}{500}\right)[1 + 0.09A^{-1/3}\phi^{-1}\left(\frac{\nu_1}{500}\right)^{1/3}], \quad (4)$$

where $A = \sqrt{\frac{m}{R_6^3}}$. Equations 4 and 3 suggest that the correlations between kHz and LF QPOs in the Alfvén wave oscillation model depend only on the two parameters, i.e., A and ϕ .

3 Results

In the general relativity precession model, we fit the relation between ν_{lf} and ν_1 with Equation 1 and the best fit is given when $m = 1.84$ and $\phi = 2.30$ with reduced χ^2 at 2.87 for 101 degrees of freedom. In this model, the lower and upper kHz QPOs are produced at the same radius, hence the same value of ϕ is used to evaluate the correlation between ν_{lf} and ν_1 . However, the best reduced χ^2 is 3.63 for 68 degrees of freedom when $m = 12.39$. On the other hand, if we simultaneously fix the m and ϕ at 1.84 and 2.30 respectively, the reduced χ^2 is as high as 13.01 for 69 degrees of freedom. Fig. 2 shows the theoretical relations between ν_{lf} and ν_2 with best consistence with the observational correlations.

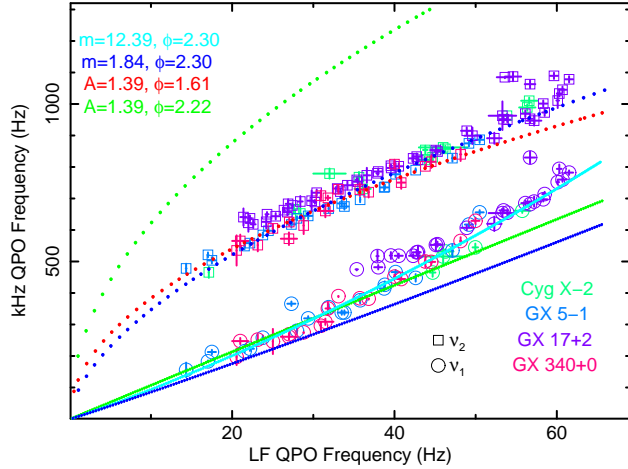


Figure 2: Fitting results for the frequency correlations between the upper kHz and LF QPOs (dotted lines) and between the lower kHz and LF QPOs (solid lines) with both the general relativity precession model and Alfvén oscillation wave model.

In the Alfvén wave oscillation model, the best fit to the observational frequency correlation between ν_2 and ν_{lf} with Equation 3 is given at $A = 1.39$ and $\phi = 1.61$ with reduced χ^2 at 3.63 for 101 degrees of freedom. Nevertheless, the fitting procedure doesn't find any minimum reduced χ^2 value when using Equation 4 to fit the correlation between ν_1 and ν_{lf} . Therefore, we fix A at 1.39 during fitting ν_1 versus ν_{lf} relation. It gives the best consistency with the observational results when $\phi = 2.22$ with reduced χ^2 of 5.60 for 68 degrees of freedom. The fitting results are also shown in Fig. 2.

In summary, although the correlations can be fitted by both models, they give non-self-consistent results. This implies that at least one of both the kHz and LF QPOs is not produced by either the general relativity precession model or Alfvén wave oscillation model. As a result, there is also another possibility: if the kHz QPOs are produced by the Alfvén wave oscillation model but the LF QPOs are not, this model of course can't explain the frequency correlations between the kHz and LF QPOs. The same possibility exists for the general relativity precession model.

References

- [1] Stella L., Vietri M., 1998, ApJL, 492, L59
- [2] Zhang C. M., 2004, A&A, 423, 401.

Energy dependence of LF QPOs for BH H1743-322 and NS Cyg X-2

Li Zhibing

Xinjiang Astronomical Observatory, Chinese Academy of Sciences, 150, Science 1-Street, Urumqi, Xinjiang 830011, China
Email: lizhibing@xao.ac.cn

1 Introduction

We investigate the energy dependence of the centroid frequency of low frequency quasi-periodic oscillation (LF QPO) of black hole (BH) H1743-322 and neutron star (NS) Cyg X-2 by using the observational data of Rossi X-ray Timing Explorer (RXTE). We find that the LF QPO frequency positively correlates with the photon energy in H1743-322 (see the left panel of Fig. 1, while inversely correlates with photon energy in Cyg X-2 (see the right panel of Fig. 1).

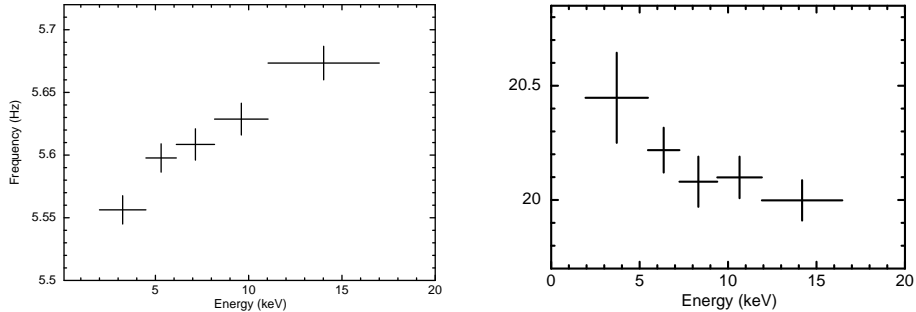


Figure 1: Energy dependence of QPO frequency. Left panel shows an example of H1743-322 while the right shows an example of Cyg X-2.

2 Interpretation

This difference suggests that the different types of QPO frequency versus photon energy relation in BH and NS may be due to the extra radiation from the NS surface, which leading to the corona temperature increasing with radius and hence an negative correlation between QPO frequency and photon energy.

振荡驱动的脉冲星辐射

林梦翔 (*Mengxiang Lin*)
北京大学物理学院天文学系
中国 北京 100871
Email: uulinm97@163.com

1 引言：转动供能脉冲星

脉冲星由于有辐射而被人发现、研究，但脉冲星的辐射机制一直是一个未被解决的问题。特别是一些特殊的爆发现象（如Giant Flares）更是令人头疼。

传统的转动供能提供了一个脉冲星辐射的简单图像，认为脉冲星是一个旋转着的导体球，同时具有偶极磁场，且磁轴方向与自转轴之间通常有一夹角 (Ruderman & Sutherland 1975)。伴随着脉冲星的自转，垂直自转轴的磁场分量产生磁偶极辐射。而平行自转轴的磁场分量也会由于自转，通过单极感应在脉冲星表面产生强电场，并且有GJ电荷密度的如下定义：其产生的电场能完全抵消单极感应所产生的电场，记为 ρ_{GJ} 。在电荷分布偏离 ρ_{GJ} 的区域，电场将把带电粒子（主要是电子）加速至极端相对论性，从而产生辐射（同步辐射、曲率辐射等）。辐射出来的一部分光子将通过量子电动力学过程转变为正负电子对，正负电子对又被电场加速，从而产生“雪崩放电”。在这个过程中，实际上是提取了脉冲星的转动动能作为辐射的能量。

2 振荡驱动

如果脉冲星在某些情况下产生振荡（比如星震所激发的星体的自由振荡），那么其振荡将在一定程度上扮演与脉冲星自转相似的角色。振荡过程中，单极感应效应仍起作用，将在脉冲星表面感生出交变的强电场。类似于转动供能中的 ρ_{GJ} ，也能给出振荡所对应的 ρ_{GJ} (Zanotti et al. 2012)

$$\rho_{GJ,osc} = -\frac{1}{4\pi c} \frac{1}{R\eta^4} \frac{B_0 e^{-i\omega t}}{\Theta^2(\eta)} \frac{1}{N} \frac{f(\eta)}{f(1)} \tilde{\eta}(1) l(l+1) Y_{lm}. \quad (1)$$

上式中的结果依赖于一些脉冲星的基本参量及振荡的模式与幅度，并且这里已经将广义相对论效应考虑在内。重要的是，其对应的电场与转动感生的电场作用相似，可将带电粒子（主要是正负电子）在极短时间内加速至极端相对论性，并通过辐射光子将电子的能量带走。所以尽管振荡产生的电场是交变的，仍然会有辐射产生。已有的计算表明，振荡感生的电场强度与自转所产生的电场强度可比，甚至

在某些条件下远大于自转产生的电场强度（具体依赖于脉冲星参数以及振荡的幅度和模式），相应地也将产生更强的辐射。

在这个过程中，提取的是星体振荡的能量。而星体振荡的能量本质来源于脉冲星的引力势能的释放（如果认为是星震激发了振荡）。振荡驱动可以与转动驱动同存在，为脉冲星的辐射供能。

3 总结与展望

脉冲星辐射的能量来源一直是一个很重要的问题，振荡驱动作为与转动驱动平行的一种模式，也可以作为脉冲星产生的辐射的一种机制，而其能量本质上来源于引力势能的释放。考虑到星体的振荡可能来源于星震，或可借此来理解Glitch中某些爆发现象。具体过程还有待进一步研究。

References

- [1] Ruderman M. A. & Sutherland P. G., *Astrophys. J.*, 1975, 196, 51
- [2] O. Zanotti, V. Morozova, & B. Ahmedov, *A & A.*, 2012, 540, A126

回落盘的制动：从射电脉冲星到磁星

刘雄伟 (*Xiongwei Liu*)
西华师范大学物电学院
北京大学物理学院天文学系
中国 南充 637002
Email: xiongwliu@163.com

1 引言：一颗向磁星区域演化的射电脉冲星

对反常X射线脉冲星（AXPs）的一种解释是磁星理论，即认为它们是一诞生就具有超强磁场的脉冲星，靠磁场能量提供明亮的X射线光度。另一种解释是回落盘供能，即认为它们是普通射电脉冲星，靠吸积回落盘的物质提供能量。如果AXPs是磁星，与普通射电脉冲星就没有什么联系，如果它们是吸积供能的，就应该与普通射电脉冲星有一定联系。

射电脉冲星J1734-3333在 $P - \dot{P}$ 图上的位置处于普通射电脉冲星和AXPs之间，并且通过13.5年持续的监测发现它正朝着AXPs所在的区域演化（制动指数 $n = 0.9 \pm 0.2$ (Espinoza et al. 2011)）。按照已知的理论，一颗正常的脉冲星不可能有这样的演化方向，因此这颗脉冲星可能有我们未知的原因。一种观点认为它是一颗潜在的磁星，即认为部分磁星在刚诞生时磁场可能被回落物质埋在了脉冲星内部，而后又慢慢释放出来，磁场强度不断增强，从而呈现出观测到的演化方向。这种解释实际上是对传统的磁星理论做了一定修改，使射电脉冲星和磁星有了联系。我们认为，如果在J1734-3333的周围存在一个回落盘，回落盘的制动作用也可以使得它向AXPs的方向演化。

2 回落盘的制动：从射电脉冲星到磁星

如果一颗脉冲星周围存在盘，盘将会和脉冲星的磁场发生作用，产生一个额外的制动力矩。力矩的大小和脉冲星的自传频率、磁场强度、以及盘的吸积率都有关。在我们的模拟中，采用了普通的自相似盘模型，即盘的吸积率随时间指数衰减（ $\dot{M} \propto t^{-\alpha}$ ）。在考虑到盘物质的动能密度和磁场磁能密度的竞争后，我们提出了一个新的修正的制动力矩，即

$$N = 2\dot{M}R_m^2\Omega_K(R_m)\left\{1 - \left[\frac{\Omega}{\Omega_K(R_m)}\right]^\chi\right\}, \quad (1)$$

其中修正因子 $0 < \chi < 1$ 。修正的力矩比文献中出现过的 $\chi \geq 1$ 的力矩强度要弱一些。拟合结果见图1，详细信息请见Liu et al. (2012)。我们尝试了 $\chi = 1/2$ 和 $\chi =$

$1/3$ 两种修正的力矩，结果都可以使J1734-3333通过现在的位置，并且其演化方向与观测一致。作为对比，我们也尝试了 $\chi = 1$ 和 $\chi = 2$ 两种力矩，结果是在通过现在的位置时都无法拟合出观测到的演化方向。

用 $\chi = 1/2$ 和 $\chi = 1/3$ 两种力矩拟合时，所需的脉冲星磁场强度仅为 $\sim 10^{12}$ 高斯，比J1734-3333按磁偶极制动计算出的磁场小大约一个量级。盘的制动可以使这颗脉冲星在大约两万年后演化到AXPs区域。当它进入AXPs区域时，剩余盘的质量大约为10个地球质量，这与在AXP 4U 0142+61周围观测到的盘的质量相当。目前这颗星与盘的作用处于螺旋桨相，吸积物质无法到达脉冲星表面就被抛到了外面，因此可以观测到射电辐射。当这颗星进入AXPs区域的时候，盘与星的作用进入跟踪相，盘物质可以掉到星表面，盘在那时的吸积率为 $\sim 10^{14} \text{ g/s}$ ，吸积物质掉到星体表面产生的X射线光度正好是典型的AXPs的光度。

3 总结

回落盘对脉冲星产生一个额外的制动力矩，使得脉冲星的演化在 $P - \dot{P}$ 图上有了不同寻常的轨迹，当盘物质可以被脉冲星吸积到表面的时候，又可以自然的产生明亮的X射线光度。这勾勒出一颗射电脉冲星演化成AXP的一幅自治的图像。在这个图像中，脉冲星J1734-3333可能正处在演化的中间环节。

References

- [1] Espinoza, C. M., Lyne, A. G., Kramer, M., Manchester, R. N., & Kaspi, V. M. 2011, ApJ, 741, L13
- [2] Liu, X. W., Xu, R. X., Qiao, G. J., Han, J. L., & tong, H. 2012, arXiv:1211.4185, accepted by RAA

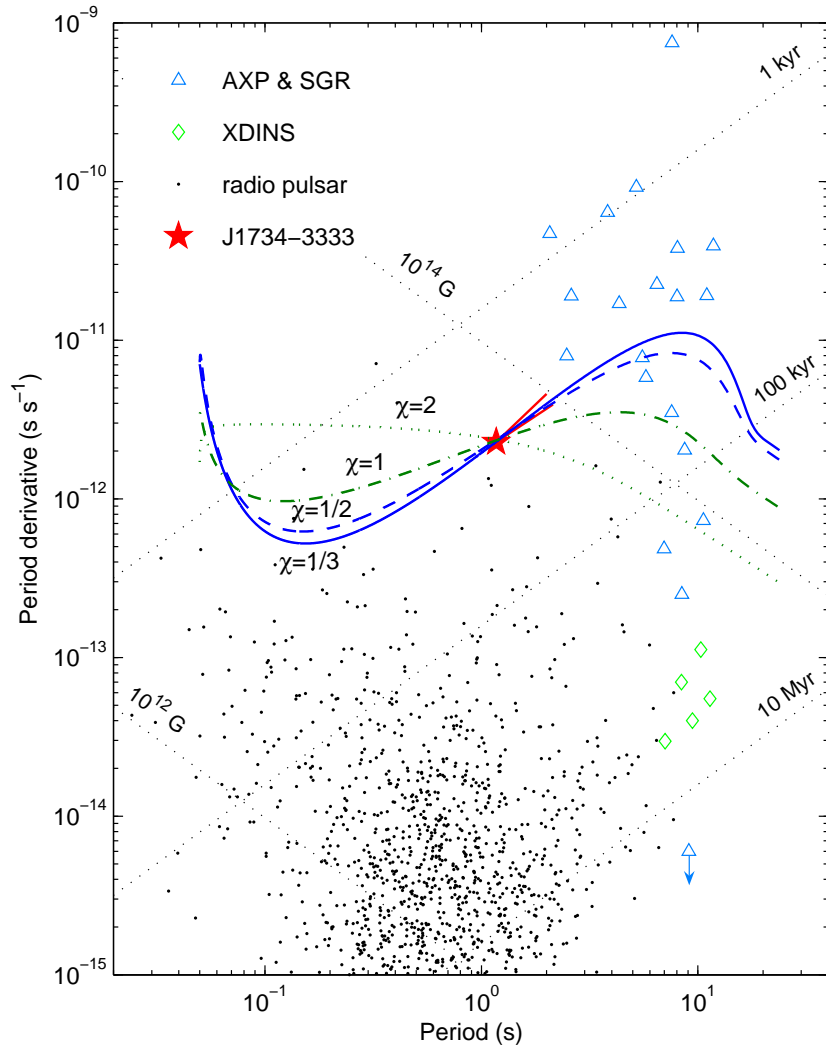


Figure 1: 一颗脉冲星在回落盘的制动力矩作用下在 $P - \dot{P}$ 图上的演化轨迹. 其中假设脉冲星初始周期 $P_0 = 50$ ms. 两根红色线段标出了观测值的误差范围。 $\chi = 1/2$ 和 $\chi = 1/3$ 两种力矩都可以同时拟合出脉冲星的位置和演化方向, $\chi = 1$ 和 $\chi = 2$ 两种力矩在拟合出位置后不能同时拟合出演化方向。拟合中所采用的磁场强度和盘质量等参数都是常规值, 具体细节请见 Liu et al. (2012).

通过X射线偏振辨别脉冲星结构模型

卢吉光 (*Jiguang Lu*)
北京大学物理学院天文学系
中国 北京 100871
Email: lujig@pku.edu.cn

1 脉冲星结构模型

1932年L. Landau提出的大原子核模型可以认为是中子（强子）星模型的始祖。通过中子星模型能够解释很多脉冲星现象，同时也有很多关于中子星内部结构的相关模型被提出，这中间也包括在中子星核心区存在夸克物质相的混合星模型。随着渐近自由理论的提出，夸克星也成为一种可能的模型。不过夸克在何种密度下才会成为自由态尚属于一个有争议的问题。也有可能夸克会汇聚成为一个个类似强子的集团，这样的模型可以称为夸克集团星模型。图 1示意了不同的脉冲星结构模型。目前尚无切实可信的证据证实或证伪这些模型。



Figure 1: 不同类型的脉冲星结构模型。其中强子星和混合星是引力束缚的，拥有由原子核和电子气等组成的壳层；夸克星和夸克集团星的表面是自束缚的，原则上表面可以为直接裸露的夸克。

2 脉冲星的热辐射X射线偏振

一般来说，可能改变脉冲星表面热辐射偏振度的机制有三种。

第一种是由于脉冲星表面的温度梯度造成的偏振。脉冲星表面的热辐射光子依据辐射电场方向是平行于还是垂直于脉冲星磁场方向与波矢方向组成的平面，可以分为O模光子与E模光子。E模光子的自由程远大于O模光子的自由程。而处于冷却过程中的脉冲星表面必存在一个指向星体内部的温度梯度。这使得E模光的热温度（强度）要高于O模光的热温度（强度），偏振就此产生。理论模型计算表明带壳层的中子星模型给出的偏振度高于10%。除此之外，真空共振效应以及强磁场下的真空双折射效应都会影响出射光的偏振，计算表明它们都会带来较高的偏振度。

3 夸克（集团）星致密表面的特殊偏振性质

对于夸克（集团）星而言，因表面没有由普通物质构成的壳层，而是直接暴露的致密物质，其物理性质与一般中子星不同。

相比于中子星的壳层，夸克星表面的物质密度要高许多，这使得真空共振效应很难发生。在夸克星（集团）模型中，不需要类似于磁星模型的强磁场便可以解释AXP与SGR的一些特性，因此强磁场下的真空双折射效应也不需要考虑。

温度梯度导致的热辐射偏振在夸克（集团）星模型与中子星模型中也存在着不同。夸克星表面的电子简并度更高，电子的平均自由程的增加使热导率更高，降低了温度梯度与偏振度。另一方面，高的电子简并度会增加光子的自由程，光深的增加会使E模光与O模光的热温度差增大，偏振度增加。同时，高的电子简并度使电子能量变高，光子与电子间的碰撞散射截面会变小，这同样会使光子自由程变长。除此之外，电子密度的增加以及强子相对数目的增加同样会影响光子的自由程。以上因素都会影响偏振度，偏振度具体是增加还是减小必须经过计算得出。

我们的计算表明，夸克（集团）星的热辐射偏振度 $P \leq 10^{-4} \%$ （见图 2），这样低的偏振度几乎无法测量。因此可以用X射线偏振探测来辨别脉冲星的中子星模型与夸克星模型，同样也可以辨别AXP & SGR的磁星模型与夸克星模型。

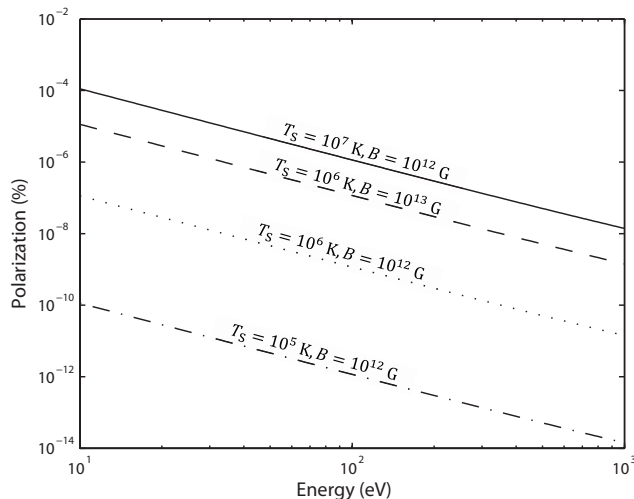


Figure 2: 对于不同温度与磁场强度的夸克集团星发出的热辐射的线偏振度。

References

- [1] Lu, J. G., Xu, R. X. & Feng, H. 2013, Chin. Phys. Lett. 30, 059501

How to check the pulsar radio radiation models observationally?

Guojun Qiao

Department of Astronomy,

School of Physics

Peking University

Beijing 100871

P. R. China

Email: gjn@pku.edu.cn;

Cooperators: K.J. Lee, Y.J. Du, X.W. Liu, J.G. Lu & R.X. Xu

Abstract

At present in our country 25m, 40m and 65m radio telescopes can be used to observe pulsars. FAST can observe after 2016. How can we use these telescope better. Here we suggest a way to check the telescopes and pulsar radiation models at the same time, that is a pulsar average pulse profile observing.

1 Introduction

FAST will play a very important role in pulsar research. Which will find more pulsars, may be find a sub-millisecond pulsar sa well as a pulsar- black hole binary. Beside these, it will play a very important role in finding radiation locations & acceleration locations of pulsars, to take check for radiation mechanisms observationally.

Pulsars have been found more than 40 years. Observations from radio to gamma-rays present abundant information. However, the radiation mechanism is still an open question. “Observed” radiation locations and its related properties are a key point to distinguish the acceleration and radiation models. 25m, 40m & 65m telescopes, especially the FAST could present a chance for us to do that. One can take Gauss fitting for the multi-frequencies observation light curves, then find the radiation locations as well as radiation locations change with frequencies. In this way, can find which model is better and which one is’nt. So from this fitting we can obtain valuable information of radiation locations.

2 An example

Our suggestion as it was done for PSR B2111+46 by Zhang et al.(2007). First of all Component-separation by Gaussian fitting to pulse profiles of PSR B2111+46 at several frequencies. An example is showing in Fig.1. Then to take three-dimensional calculations of the pulsar emission height. The observed points get from Gaussian fitting and calculated points of the pulsar emission height are showing Fig.2. This is a very important way to check the radiation models.

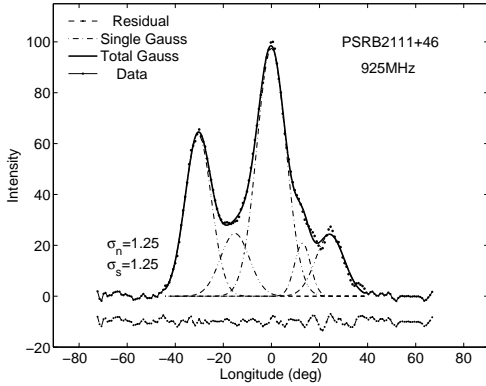


Figure 1: Component-separation by Gaussian fitting to profiles of PSR B2111+46.

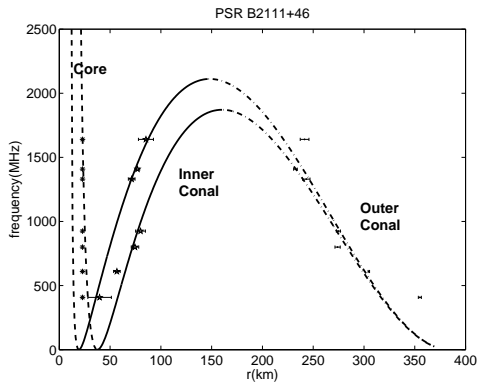


Figure 2: The data points were calculated at the field lines footed at 75% of the polar cap radius by taking $\alpha = 9^\circ$, $\beta = 1.4^\circ$ from Rankin (1993). Two curves were calculated for the two sparking points at 74% of polar cap radius in the $\Omega - \mu$ plane for the ICS model (Qiao & Lin 1998) with a linear decay of the Lorentz factor as $\gamma = \gamma_0(1 - \kappa \frac{r-R}{R_e})$, and $\gamma_0 = 10000$ and $\kappa = 225$.

3 Conclusion and discussion

Here it is focus that: 1. How to check the telescopes at the beginning; 2. What kind of observations is simple; 3. The simple observations are meaningful and can be published?

References

- [1] G. J. Qiao & W. P. Lin, A & A., 1998, 333, 172
- [2] J. M. Rankin, 1993, ApJS, 85, 145
- [3] H. Zhang, G. J. Qiao, J. L. Han, K. J. Lee, and H. G. Wang, A & A., 2007, 465, 252

SGR短爆能量来源

屈稚杰 (*Zhijie Qu*)
北京大学物理学院天文学系
中国 北京 100871
Email: quzhijie@pku.edu.cn

1 引言：当前SGR研究中的问题

SGR(soft gamma repeater)是一类十分特殊的脉冲星。目前已经发现的SGR共有十余颗，在浩瀚的宇宙中应该说是非常稀少的。它们有一些共同的特殊性质，比如较长的周期 P ，以及较大的周期演化 \dot{P} 。此外它们还有被称为爆发期(outburst)的现象。在爆发期中，SGR会有较大流量的X射线持续辐射，并且还有被称为短爆的(short burst)的爆发。这种短爆的时标较短，并且可以达到较高的能段。

但是现在人类对于SGR的这些特殊性质的理解并不深刻，这一方面是因为SGR发现较晚且数量较少，但另一方面，更严重的原因是SGR的表现与人类已有的认识有一定背离。比如，对于X射线脉冲星的研究告诉我们，X射线脉冲一般在双星系统中，辐射的主要能量来源是从伴星吸积时释放的引力能。但是SGR都是孤立的天体，所以它的X射线辐射的能量来源就有很多不同的认识。现在比较流行的看法是，它的能量来源是星体磁场的衰减。此外，也有能量来源于回落盘的吸积的解释。与此类似，短爆的能源来源也有多种解释，比如磁重联过程，星震释放弹性能，还有建立在吸积模型上的热核反应过程。

2 短爆来源于热核反应的可能性

热核反应导致爆发最典型的例子是X射线爆发(X-ray burst)。这是一种来源于低质量X射线双星(LMXB)的现象。它表现出有两种形式的爆发，Type I型爆发一般认为是源自热核反应，Type II型爆发一般认为源自吸积盘的不稳定性。由于，SGR与X射线爆发在现象的表现形式上有很多的共性。并且SGR吸积的问题在回落盘模型中也有了比较充分的讨论。所以，将SGR与X射线爆发类比也是很自然的事。

相比来说，Type I型爆发形式与SGR中的短爆更为接近。这一方面是因为SGR的回落盘吸积的吸积率是比较低的，不太可能产生较强短爆那么强的爆发；另一方面，Type II型爆发时标一般较长，与SGR短爆 $\sim 0.1s$ 的持续时间不太相符。

虽然说SGR的短爆与Type I型爆发有很多相似性，但是也有很多需要解决的问题。比如，即使是Type I型爆发，它的时标也是要比SGR短爆长的；还有，Type I型爆发的强度比较稳定，而SGR短爆的强度则差异很大；此外还有一个很根本的问题，SGR具有X射线脉冲，这被认为是表面磁场较强，这与热核反应所要求的弱磁场($\leq 10^{10} \sim 10^{11}$)是有矛盾的。

3 总结

对SGR的短爆的研究还有很多问题没有解决，它们的能量来源就是其中很重要的一个。我们期待热核反应能成为解决这个问题可能的路径中的一个。

磁星辐射机制研究

仝号 (*Hao Tong*)
中国科学院新疆天文台
新疆乌鲁木齐 830011
Email: tonghao@xao.ac.cn

我们主要从事脉冲星的理论研究，特别是磁星（magnetar）及相关脉冲星类天体。 我们主要想解决磁星3 + 1方面的问题：

1. 磁星和通常的脉冲星类天体的磁场起源；
2. 磁星的多波段辐射机制是什么？磁星现在已经有射电，光学、红外，软X射线，硬X射线等波段的观测。
3. 磁星和周围环境的相互作用。周围环境包括：可能的回落盘（fallback disk），脉冲星风云，超新星遗迹， 以及如果一颗磁星位于一个双星系统中的问题。
4. 磁星和其他脉冲星类天体的关系。其他脉冲星类天体包括：X射线暗的孤立中子星，超新星遗迹的中心致密天体， 强磁场脉冲星， 以及正常的脉冲星。

我们以研究磁星的制动机制和多波段辐射特性作为切入点，研究磁星问题。近年来我们在这一块有 若干工作，文章列表见：

<http://www.escience.cn/people/tonghao/paperlist.html>
更多内容可以访问我的个人主页。

kHz QPO对中子星的质量半径估计

王德华^{†,‡}, 陈黎[†], 张承民[‡]

[†]北京师范大学 天文系

中国 北京 100875

[‡]中国科学院国家天文台

中国 北京 100012

Email: huazai05105220@163.com

1 引言

千赫兹准周期震荡(kHz QPO)是中子星低质量X射线双星(NS-LMXB)特有的一种时变性质。它表现为功率谱上的双峰, 分别对应上频 $\nu_1(\sim 700 \text{ Hz})$, 下频 $\nu_2(\sim 1000 \text{ Hz})$ 。目前较符合观测的理论模型包括相对论进动模型[11](RPM)和阿尔文波震荡模型[17](AWOM)。其中阿尔文波模型认为双kHz QPO的上频是物质运动的开普勒轨道频率, 而下频是磁流体力学的阿尔文波震荡频率, 模型的自由参数是中子星密度。此模型可以用来限制中子星的质量半径($M - R$)关系[18]。本文收集具有测量质量和双kHz QPO的中子星低质量X射线双星数据, 应用阿尔文波震荡模型, 限制这些源的中子星 $M - R$ 关系, 进而限制中子星的内部物态。

2 模型

阿尔文波震荡模型:

$$\nu_2 = \sqrt{\frac{GM}{4\pi^2 r^3}} \quad (1)$$

$$\nu_1 = 629(\text{Hz}) A^{-2/3} \nu_{2k}^{5/3} \sqrt{1 - \sqrt{1 - (\frac{\nu_{2k}}{1.85A})^{2/3}}} \quad (2)$$

$$A = \sqrt{\frac{m}{R_6^3}} \quad (3)$$

$$\rho = 4.75 \times 10^{14} A^2 (\text{g cm}^{-3}) \quad (4)$$

其中 M 为中子星质量(m 是以 M_\odot 为单位的中子星质量), $\nu_{2k} = \nu_2/1000 \text{ Hz}$, $R_6 = R/10^6 \text{ cm}$ 为中子星半径, A 等价于中子星的密度参数。

Table 1: 具有测量质量和双kHz QPO的NS-LMXB源

源 (3)	测量质量 (M_{\odot})	ν_1 (Hz)	ν_2 (Hz)	A	参考文献
Cyg X-2	1.78 ± 0.23 1.5 ± 0.3	516 ± 27	862 ± 11	0.62 ± 0.04	[8, 13] [5, 13]
SAX J1808.4-3658	< 1.4	$499 \pm 4 \sim 503.6 \pm 5.3$	$685.1 \pm 5.1 \sim 694 \pm 4$	0.43 ± 0.01	[4, 12, 14]
4U 1820-30	$1.29^{+0.19}_{-0.07}$	$764 \pm 6 \sim 796 \pm 4$	$1055 \pm 10 \sim 1072 \pm 11$	0.65 ± 0.01	[9, 10]

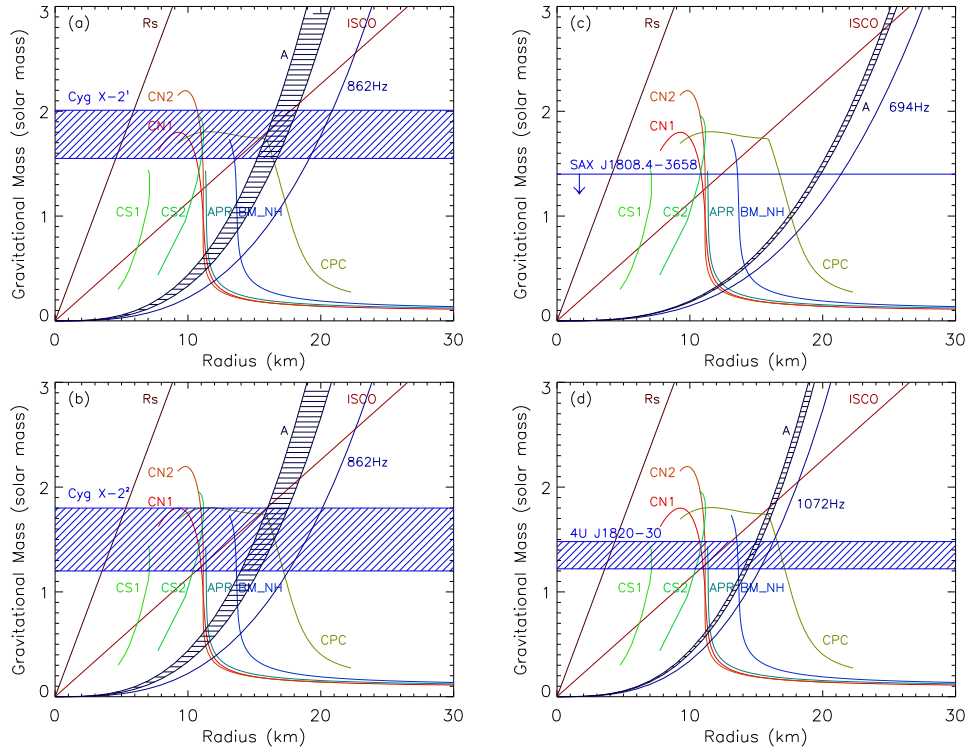


Figure 1: 中子星 $M - R$ 图。EOS曲线(见[1, 2, 7]): a.中子星包含奇异夸克物质(CS1 and CS2), b.仅包括核子[1](APR), c.包括核子和重核[2](BM_NH), d.由正常中子物质组成(CN1、CN2), e.含有致密介子核[6, 3](CPC)。 R_s 为施瓦希半径, ISCO为最小稳定轨道半径。

3 结果与讨论

我们根据阿尔文波震荡模型和双kHz QPO数据，计算得到模型参数 A (等价于中子星密度)。在 $M - R$ 图上，我们根据测量到的中子星质量和AWOM 预言的密度参数 A ，限制出中子星的 $M - R$ 范围，并与理论预言星体状态方程曲线(EOS)相比较，从而判断该中子星可能的物态。从图中可看出Cyg X-2的中子星可能包括致密介子核(CPC)；SAX J1808.4-3658的中子星物态应排除奇异夸克物质[15, 16](CS1和CS2)；4U 1820-30的中子星可能包括致密介子核或者核子与重核子核(BM_NH)。

References

- [1] Akmal A., Pandharipande V. R., Ravenhall D. G., 1998, Phys. Rev. C, 58, 1804
- [2] Bednarek I. et al., 2012, A&A, 543, A157
- [3] Cook G. B., Shapiro S. L., Teukolsky S. A., 1994, ApJ, 424, 823
- [4] Elebert P. et al., 2009a, MNRAS, 395, 884
- [5] Elebert P. et al., 2009b, MNRAS, 395, 2029
- [6] Lattimer J. M., Prakash M., 2001, ApJ, 550, 426
- [7] Miller M. C., 2002, Nat, 420, 31
- [8] Orosz J. A., Kuulkers E., 1999, MNRAS, 305, 132
- [9] Shaposhnikov N., Titarchuk L., 2004, ApJ, 606, L57
- [10] Smale A. P., Zhang W., White N. E., 1997, ApJ, 483, L119
- [11] Stella L., Vietri M., 1999, Phys. Rev. Lett., 82, 17
- [12] van Straaten S., van der Klis M., Wijnands R., 2005, ApJ, 619, 455
- [13] Wijnands R. et al., 1998, ApJ, 493, L87
- [14] Wijnands R. et al., 2003, Nat, 424, 44
- [15] Xu R. X., 2009, Journal of Physics G: Nuclear and Particle Physics, 36, 064010
- [16] Xu R. X. et al., 2012, Phys. Rev., 85, 023008
- [17] Zhang C. M., 2004, A&A, 423, 401
- [18] Zhang C. M. et al., 2007, Astron. Nachr., 328, 491

Understanding Isolated And Accreting Magnetars In Hard X-rays

Wei Wang

National Astronomical Observatories

Chinese Academy of Sciences

Beijing 100012

P. R. China

Email: wangwei@bao.ac.cn

1 Introduction

Magnetars are a special class of neutron stars with an ultra-strong surface magnetic field of higher than $\sim 4.4 \times 10^{13}$ G. Anomalous X-ray pulsars (AXPs) and soft gamma-ray repeaters (SGRs) emitting X-rays with luminosities much higher than their spin-down power involve the idea proposal of magnetars (Thompson & Duncan 1996). No companions and obvious accreting features are discovered in the systems of AXPs and SGRs, which leads to the support of the magnetar assumption. So that AXPs and SGRs are suggested to be the isolated magnetars, and X-ray emissions come from the magnetic field activities or decay of the strong magnetic field. Recently some superslow pulsation X-ray pulsars are discovered in some high mass X-ray binaries (HMXBs). These neutron star systems are difficultly produced in present standard evolution scenario of close neutron star binaries except that we assume the neutron stars in binaries have a strong magnetic field, e.g., higher than $\sim 10^{14}$ G. Thus we define these superslow pulsation X-ray pulsars as accreting magnetars. In this paper, we will mainly review the hard X-ray observational results and progress on both isolated and accreting magnetars. The hard X-ray observations will help us to understand the radiation mechanism of magnetars, formation scenario and evolution of magnetar systems.

2 Hard X-ray Characteristics of Isolated Magnetars

Isolated magnetars generally have the following observed features: spin period in the range of 2-12 seconds; young characteristic age (10-100 kyr); some AXPs and SGRs are associated with supernova remnants; an inferred dipole magnetic field of $10^{14}-10^{15}$

G; persistent X-ray luminosity (0.1-10 keV) in the range of $10^{34} - 10^{36}$ erg s $^{-1}$ which is higher than their spin-down power; in the soft X-ray band of 0.1 – 10 keV, they have very soft spectra, a thermal spectrum of $kT \sim 0.35 - 0.6$ keV, or the power-law photon index $\Gamma \sim 2 - 4$; while in the hard X-ray band above 10 keV, a very hard spectrum of power-law photon index $\Gamma \sim 0.5 - 1$ is discovered; the absence of massive companion stars.

The non-thermal emission properties above 10 keV for AXPs and SGRs are still not quite well understood. The spectra of a power-law photon index $\Gamma \sim 0.5 - 1$ are reported by RXTE/PCA (Kuiper et al. 2006) and Swift/BAT (Wang 2008). However, we do not know if the power-law hard spectra will extend to above 1 MeV or have a high energy cutoff around several hundred keV. The Swfit/BAT data on 1E 1841-045 and 4U 0142+614 suggested a possible high energy cutoff around 100 keV (Wang 2008). This issue still needs high sensitivity observations.

INTEGRAL/IBIS is a high-sensitivity soft gamma-ray imager which has a 12' (FWHM) angular resolution and arcmin source location accuracy in the energy band of 15 – 200 keV. Using the long-term observations from 2003 – 2011 by IBIS, we obtained the hard X-ray spectrum from 18 – 500 keV of 4U 0142+614 which is the brightest one of all AXP sources in X-ray band. In Fig 1, we presented the hard X-ray spectrum of 4U 0142+614 fitted with a power-law model plus a high energy cutoff. The derived power-law photon index is $\Gamma \sim 0.45 \pm 0.22$, the cutoff energy $E_{\text{cutoff}} \sim 115.6 \pm 17.5$ keV. The flux from 18 – 100 keV is determined to be $\sim 1.2 \times 10^{-10}$ erg cm $^{-2}$ s $^{-1}$, corresponding to a hard X-ray luminosity of $\sim 10^{35}$ erg s $^{-1}$ assuming a distance of 3 kpc.

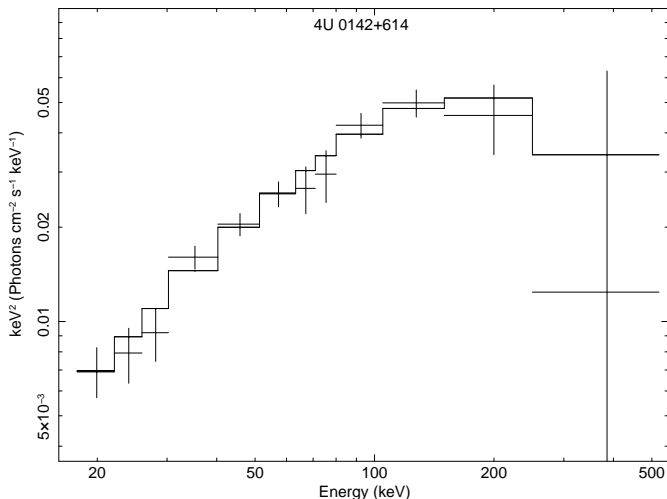


Figure 1: The hard X-ray spectrum of 4U 0142+614 from 18 – 500 keV obtained by INTEGRAL/IBIS. The spectrum shows a high energy cutoff around 100 keV.

3 Characteristics of Accreting Magnetars

High mass neutron star X-ray binaries generally are divided into two classes: Be/X-ray pulsars, the transient X-ray sources with main-sequence star companions; supergiant binaries, persistent X-ray emitters with supergiant star companions. The spin period of neutron stars in these sources generally distributes from 0.1 – 1000 s. Recently, some superslow pulsation X-ray pulsars are discovered in HMXBs with hard X-ray surveys. In Fig 2, the Corbet diagram for high mass X-ray binaries shows four superslow pulsation X-ray pulsars: 4U 2206+54 with $P_{\text{spin}} \sim 5560$ s (Wang 2009, 2010) and an orbital period of 19.12 days (Wang 2009); 2S 0114+65 with $P_{\text{spin}} \sim 9600$ s (Wang 2011) and an orbital period of 11.59 days (Crampton et al. 1985); IGR J16418-4532 with $P_{\text{spin}} \sim 1246$ s and $P_{\text{orb}} \sim 3.7$ days (Walter et al. 2006); and SXP 1062 with $P_{\text{spin}} \sim 1062$ s and $P_{\text{orb}} \sim 300$ days (Haberl et al. 2012).

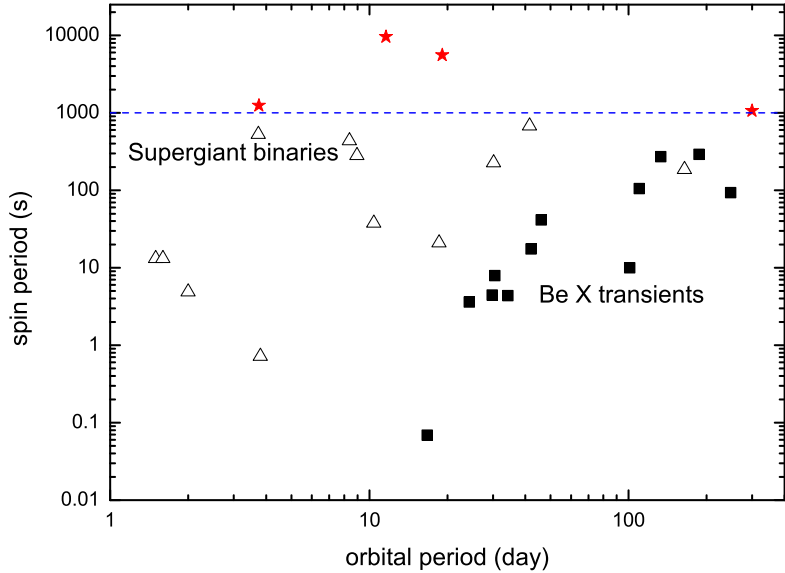


Figure 2: The spin period - orbital period diagram for the accreting X-ray pulsars in high mass X-ray binaries. Four superslow pulsation X-ray pulsars with $P_{\text{spin}} > 1000$ s is noted as stars.

In addition, long-term X-ray monitoring observations on these sources discover that they undergo fast spin-up/spin-down trends. In Fig 3, the spin period evolution of three superslow pulsation X-ray pulsars is displayed. 2S 0114+65 is a persistent X-ray source with a possible supergiant companion. It undergoes a long-term spin-

up trend in the last twenty years, and the present spin-up rate is determined to be $\sim 10^{-6}$ s $^{-1}$. And its spin-up trend seems accelerating in last 20 years. 4U 2206+54 as a peculiar X-ray binary, shows persistent X-ray emissions with a main sequence star companion. The neutron star continuously spins down in the last ten years with a mean spin-down rate of 4.9×10^{-7} s s $^{-1}$ by different measurements (Wang 2010, 2013; Finger et al. 2010; Reig et al. 2012). SXP 1062 located in the Small Magellanic Cloud is associated with a supernova remnant (age of $(2-4) \times 10^4$ yr). It belongs to a Be/X-ray pulsar which shows transient outbursts. During an outburst in 2010, it showed a large spin-down rate of 3×10^{-6} s s $^{-1}$ (Haberl et al. 2012). In 2012, another outburst was detected (Sturm et al. 2013), and from 2010 – 2012, the average spin-down rate of $\sim 10^{-7}$ s $^{-1}$ was found.

Why special for superslow pulsation X-ray pulsars?

The spin period evolution of the new-born neutron star generally undergoes three states (Bhattacharya & van den Heuvel 1991): an *ejector state* in which neutron star spins down through the conventional spin-powered pulsar energy-loss mechanisms; a *propeller state* in which spin period decreases by means of interaction between the neutron star magnetosphere and stellar wind of the companion; and an *accretor state* in which the spin period of neutron star reaches a critical value, and the neutron star begins to accrete materials on to the surface, then switches on as the X-ray pulsar. The critical period is defined by equating the corotational radius of the neutron star to the magnetospheric radius, which induces the longest period of several hundred seconds but less than ~ 1000 s for the neutron star of magnetic field $B < B_{\text{cr}} = 4.4 \times 10^{13}$ G. Then what physical channels produce the superlong spin period higher than 1000 s?

Li & van den Heuvel (1999) have suggested that neutron star spins down to the spin period range longer than 1000 s if the neutron star was born as a magnetar with an initial magnetic field $\geq 10^{14}$ G. This ultra-strong magnetic field could decay to the normal value ranges of $10^{12} - 10^{13}$ G within a few million years.

The alternative suggestion proposed by Ikhshanov (2007) shows that an additional evolution phase *subsonic propeller* state between the transition from known *supersonic propeller* state to *accretor* state could allow the spin period increases up to several thousand seconds without the assumption of magnetars, which is the so-called break period given by:

$$P_{\text{br}} \simeq 2000 \frac{M_{\text{NS}}}{1.4M_{\odot}}^{-4/21} \left[\frac{B_{\text{surf}}}{0.3B_{\text{cr}}} \right]^{16/21} \left[\frac{\dot{M}}{10^{15} \text{gs}^{-1}} \right]^{-5/7} \text{s}, \quad (1)$$

where B_{surf} is the surface magnetic field of the neutron star. However, if the above formula is applied to the case of 4U 2206+54/2S 0114+65, one find the surface magnetic field higher than 10^{14} G.

The fast spin-down rate is discovered in two superslow pulsation X-ray pulsars 4U 2206+54 and SXP 1062. According to the standard evolutionary scenario, the max-

imum spin-down rate in the accretor stage is $\dot{P} \sim 2\pi B^2 R_{\text{NS}}^6 / (GMI)$, which implies $B > 10^{14}$ G for 4U 2206+54 and SXP 1062.

Recently, a new theory of quasi-spherical accretion for X-ray pulsars is developed (Shakura et al. 2012), the magnetic field in wind-fed neutron star systems is given by

$$B_{12} \sim 8.1 \dot{M}_{16}^{1/3} V_{300}^{-11/3} \left(\frac{P_{1000}}{P_{\text{orb}300}} \right)^{11/12} G. \quad (2)$$

This also gives the ultrastrong magnetic field of $> 10^{14}$ G.

Thus a magnetar is required in these X-ray binaries in present accreting and binary evolution models. These superslow pulsation X-ray pulsars should belong to a new class of compact objects – accreting magnetars.

Accreting magnetars may be located in the other new class of high mass X-ray binaries – Supergiant fast X-ray transients (SFXTs). SFXTs have X-ray luminosity above 10^{36} erg s $^{-1}$ during the outbursts, and a quiescent luminosity of $\sim 10^{32}$ erg s $^{-1}$. Some SFXTs have been identified as X-ray pulsars with spin period from tens of seconds to one thousand seconds. The nature and physical mechanisms of SFXTs are still debated. Some people think that the stellar wind is structured, and outbursts are produced by the accretion of the very dense wind clumps (int Zand 2005, Walter & Zurita 2007). The other possibility is that SFXTs have a magnetar with a slow pulsation (> 1000 s) which induces the variability (Bozzo et al. 2008).

4 Discussion

The family of magnetars now has been divided into two classes: isolated magentars and accreting magnetars. In Table 1, we summarized the main characteristics of both isolated and accreting magnetars for the comparison.

An evolutional track for the accreting magnetars are suggested (see Fig 4). There may exist the physical link among two slow-pulsation X-ray pulsars: 4U 2206+54 and 2S 0114+65 are the younger systems undergoing rapid spin period evolutions, i.e., from the spin-down phase of 4U 2206+54 to the spin-up phase of 2S 0114+65. The evolution channel from the 4U 2206+54-like system to the 2S 0114+65-like system could be supported by the their companion types: according to the evolutional tracks of massive stars (Meynet et al. 1994), the possible progenitor of a B1 supergiant in 2S 0114+65 is an O9.5 V star consistent with the main-sequence star type in 4U 2206+54. The SFXTs may be the product of 2S 0114+65-like sources which evolves to the equilibrium period less than ~ 1000 s through spin-up processes.

I am grateful to Prof. R. X. Xu for the invitation to give a presentation on magnetars in this conferences. This work is mainly based on observations of INTEGRAL, an ESA project with instrument and science data center funded by ESA member states and supported by the National Natural Science Foundation of China (No. 11073030).

References

- [1] Bhattacharya, D. & van den Heuvel, E.P.J., Phys. Rep., **203**, 1 (1991)
- [2] Bozzo, E.; Falanga, M.; Stella, L., ApJ, **683**, 1031 (2008)
- [3] Crampton, D., Hutchings, J.B., Cowley, A.P., ApJ, **299**, 839 (1985)
- [4] Finger, M. H. et al., ApJ, **709**, 1249 (2010)
- [5] Haberl, F. et al., A&A, **537**, L1 (2012)
- [6] Kuiper, L. et al., ApJ, **645**, 556 (2006)
- [7] Ikhsanov, N.R., MNRAS, **375**, 698 (2007)
- [8] in't Zand, J. J. M., A&A, **441**, L1 (2005)
- [9] Li, X.D. & van den Heuvel, E.P.J., ApJ, **513**, L45 (1999)
- [10] Maynet, G. et al., A&AS, **103**, 97 (1994)
- [11] Reig, P., Torrejón, J.M., Blay, P., MNRAS, **425**, 595 (2012)
- [12] Shakura, N. et al., MNRAS, **420**, 216 (2012)
- [13] Sturm, R. et al., arXiv:1304.6022 (2013)
- [14] Thompson, C. & Duncan, R.C., ApJ, **473**, 322 (1996)
- [15] Walter, R. et al., A&A, **453**, 133 (2006)
- [16] Walter, R.; Zurita Heras, J., A&A, **476**, 335 (2007)
- [17] Wang, W., edt. by Y. F. Yuan, X. D. Li & D. Lai, AIP Conf. Proceedings, **968**, 101 (2008)
- [18] Wang, W., MNRAS, **398**, 1428 (2009)
- [19] Wang, W., A&A, **520**, 22 (2010)
- [20] Wang, W., MNRAS, **413**, 1083 (2011)
- [21] Wang, W., MNRAS, **432**, 954 (2013)

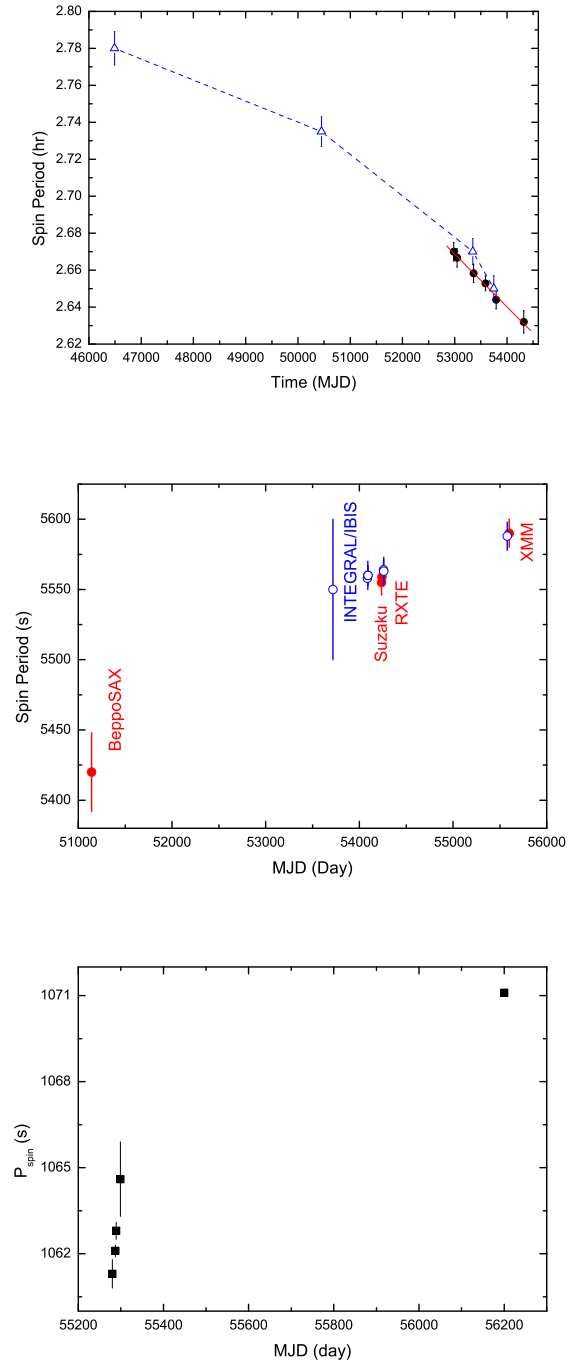


Figure 3: The spin period evolution of three superslow pulsation X-ray pulsars. **Top** Long-term spin-up trend of 2S 0114+65; **Middle** long-term spin-down trend of 4U 2206+54; **Bottom** spin-down trend of SXP 1062.

	Isolated magnetars	Accreting magnetars
Spin period (s)	2–12	> 1000
Spin period derivative (s/s)	$10^{-12} - 10^{-10}$	$10^{-7} - 10^{-6}$
Characteristic age (yr)	$10^4 - 10^5$	$10^4 - 10^6$
X-ray spectral properties	< 10 keV: thermal $kT \sim 0.1 - 1$ keV > 10 keV: non-thermal with $\Gamma \sim 0.5 - 1.5$ Cutoff energy ~ 100 keV	Power-law plus a high energy cutoff $\Gamma \sim 1.5 - 2.5$ Cutoff energy $\sim 30 - 100$ keV
X-ray luminosity (1–100 keV)	Quiescence: $10^{35} - 10^{36}$ erg s $^{-1}$ Bursts: $> 10^{40}$ erg s $^{-1}$	$10^{34} - 10^{37}$ erg s $^{-1}$
Energy power	Magnetic field decay/activity	Wind-fed direct accretion

Table 1: The comparison between isolated magnetars and accreting magnetars.

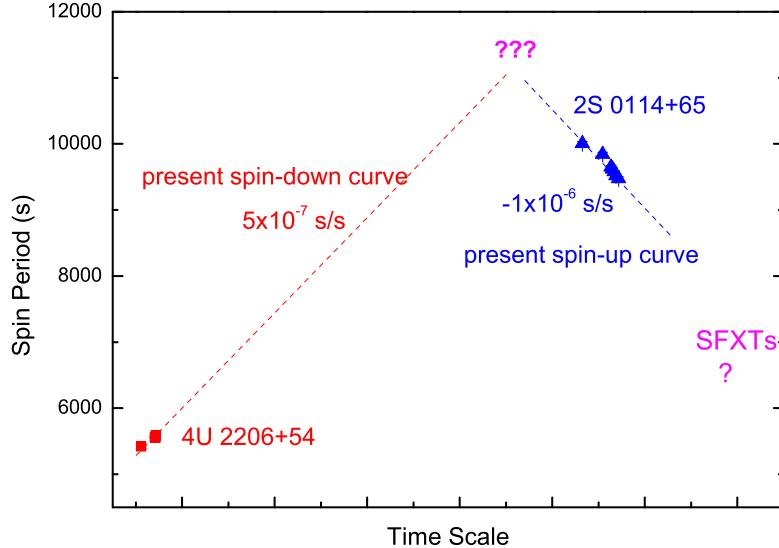


Figure 4: The imaginary picture of evolutional scenario of accreting magnetars. This cartoon picture shows the spin period evolution history of two superslow pulsation neutron stars in high mass X-ray binaries 4U 2206+54 and 2S 0114+65. 4U 2206+54 undergoes a spin-down process with a rate of $\sim 5 \times 10^{-7} \text{ s s}^{-1}$, which will make the spin period of 4U 2206+54 longer than 10000 s within 300 years if the rate is stable in next a few hundred years. While, 2S 0114+65 undergoes a fast spin-up process in the last twenty years with spin period variations from $\sim 10000 \text{ s}$ to present 9500 s. It is possible that there exists a candidate neutron star binary with a spin period much longer than 10000 s which may be the product of long-term spin down of the 4U 2206+54-like neutron star and would undergo the spin-up transition to form the 2S 0114+65-like source. This class of accreting magnetars would evolve into the next equilibrium spin period stage as the detected SFXTs.

对称能：从两味到三味？

徐仁新 (*Renxin Xu*)
北京大学物理学院天文学系
中国 北京 100871
Email: r.x.xu@pku.edu.cn

1 引言：核物理中的对称能

经验告诉我们，稳定原子核中的质子数 Z 和中子数 N 倾向于相等，尽管人们至今并未深刻地理解其中的道理。一般通过引进对称能这一概念来刻画这一观测事实，这样核子数 A ($= Z + N$) 原子核的质量表示为

$$E(Z, N) = a_v A + a_s A^{2/3} + a_{\text{sym}} \frac{(N - Z)^2}{A} + a_c \frac{Z(Z - 1)}{A^{1/3}} + a_p \Delta(Z, N),$$

其中第一项是体积能，第二项是表面能，第三项是对称能，第四项是Coulomb能，第五项是对能。单从第三项对称能表达式可见，质子数 Z 相对于中子数 N 的偏离程度越高，则原子核越不稳定（表现为质量 E 越大）。

怎么理解存在对称能这一事实呢？传统上，人们可以通过核子Fermi气图像得到类似的关系；但值得注意的是：Fermi气模型只有在相互作用比较弱时才是合理的。而问题是，原子核内核子之间的核力却比较强。另外一种理解对称能的思路或是通过考察夸克的味对称性。正如NaCl晶体中Na、Cl两类离子数目数目相同时相互作用导致的能量最低，也许原子核内的相互作用也会导致 Z 、 N 数目相等时较稳定。我们知道，核子由夸克构成，“ $Z = N$ ”等效于u、d夸克数目的相等。

容易理解对称能项将反映在物态的软硬程度上。 Z 相对于 N 越偏离，核物质内能越高，能够抵抗星体引力收缩的能力越强；这就表现为物态越硬。如果认为脉冲星是“纯中子”组成的 ($N \gg Z$)，则因对称能贡献物态显著趋“硬”。目前，随着大质量 ($\sim 2M_\odot$) 脉冲星的发现，对称能研究也理所当然地受到学界的关注。

2 压缩重子物质对称能：轻味夸克对称？

在粒子物理标准模型中，基本Fermi子包括夸克和轻子，分三代六味；其中六味夸克依质量一分为二：质量较轻的轻味夸克{u,d,s}和质量较重的重味夸克{c,t,b}。在核物质密度情形下，无论是据Heisenberg关系估计的零点能还是简单夸克Fermi气图像所给出的Fermi能都是 ~ 400 MeV，显著大于轻夸克之间的质量差($m_u \sim m_d \sim 10$ MeV，而 $m_s \sim 100$ MeV)。这就产生一个发人深省的问题：既然包括奇异夸克在内

的所有轻味夸克都容易激发产生，那么原子核为何非奇异？换言之，为何原子核系统具有的是{u,d}两味对称性（即同位旋对称性）而不是{u,d,s}三味对称性呢？

消除以上迷惑需要认清色作用远强于电磁作用这一根本事实。由夸克构成的、质量最轻的色单态是核子，质量不足940MeV；而uds三味组成的 Λ 超子质量却>1110MeV。这其中的质量差约100MeV。似乎两味对称（由核子组成）的原子核要比三味（ Λ 组成）要经济些，但为了保持电中性，伴随着核子的“小尾巴”——电子却是甩不掉的。不过，作为质量最轻的荷电轻子，电子($m_e = 0.511\text{MeV}$)在利用较弱的电磁作用与原子核这个强作用客体耦合在一起时，其分布范围远远超过核：局域电子相对论性运动的特征尺度Compton波长 $\sim 0.024\text{\AA} \gg$ 局域夸克（原子核）尺度 $\sim \text{fm}$ 。所以，由核子构成的原子核确实比较“经济”。这个花香鸟语的精彩世界之本质即如此。让我们庆幸色、电相互作用强度之间如此巨大的差别吧！

但是，对于超新星爆发残留的压缩重子物质——致密星而言，电子则处于其内。如果这类物质还是两味对称的，电子动能 $E_e \sim \hbar cn^{1/3}$ 也将达到 $\sim 10^2\text{MeV}$ (n 为电子的数密度)。而若大原子核具有三味对称性，则可显著降低电子对系统总能量的贡献，同时也使得味自由度尽可能大。因此，虽然原子核的对称能本质上反映了u、d两味对称，但不排除致密星相应的对称性却是三味（轻味）的。

3 总结

如果原子核与致密星的差别主要就体现在二味、三味上，则致密星内部的基本单元不太可能是三价夸克组成的强子（原因是 Λ 两体作用为吸引），很可能是H（双重子）或类似的夸克集团。这样，夸克集团星也就成为脉冲星结构的候选模型之一。

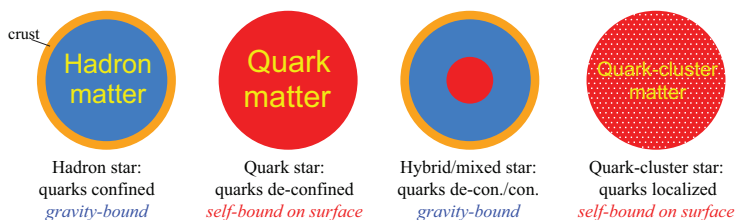


Figure 1: 不同类型的脉冲星结构模型。强子星(hadron star)内部无游离夸克组成的夸克物质，而中心密度足够高时会形成具有夸克物质核心的混合/混杂星(hybrid/mixed star)。几乎完全由夸克物质构成的致密星称为夸克星(quark star)。以夸克集团为主要自由度的夸克集团星(quark-cluster star)有别于通常的中子星和夸克星。强子星和混合/混杂星是引力束缚的，这两类致密星都拥有由原子核和电子气等组成的壳层(crust)；而夸克星和夸克集团星的表面是色作用自束缚的，原则上可以不具有壳层。表面直接裸露的夸克(集团)星称为裸夸克(集团)星。

再次重申：作者致力于发展夸克集团星模型及其观测检验；更多的研究进展请浏览个人主页：<http://www.phy.pku.edu.cn/~xurenxin/index.html>。欢迎加盟！

上海65米射电望远镜脉冲星观测研究

闫振^{[1]*}, 沈志强^[1], 吴鑫基^[2]

[1]中国科学院上海天文台, 中国 上海 200030

[2]北京大学天文系, 中国 北京 100871

*Email: yanzhen@shao.ac.cn

1 引言

脉冲星因发射具有严格周期性的脉冲信号而得名。脉冲星不仅是验证强磁场、强引力等极端条件下物理规律的空间实验室，而且也是探测引力波以及星际介质的重要探针[1, 2]。绝大多数脉冲星只在射电波段具有辐射，该波段无疑是脉冲星观测研究的重要窗口。新建的上海65米射电望远镜已经配备四个低频波段(L、S、C、X)的接收机。表1列举了上海65米射电望远镜以及国际上进行脉冲星观测研究的同类型大型望远镜的性能，其中Freq-R为接收机带宽，系统等效流量密度SEFD = $2k_B T_{sys}/A_e$ ，单位分别为GHz和Jy。对比可见该望远镜性能优异，尤其在C波段。脉冲星将是上海65米射电望远镜的重要科学目标之一。本文将介绍上海65米射电望远镜脉冲星试观测情况以及近期脉冲星观测研究计划。

	GBT[3]	Effelsberg [4]	Parkes[5]	Lovell[4]	SH65m
L	Freq-R	1.15-1.73	1.27-1.45, 1.59-1.73	1.2-1.8	1.25-1.50, 1.55-1.73
	SEFD	10	20,19	31	36,65
S	Freq-R	1.73-2.6	2.20-2.30	2.2-2.5	—
	SEFD	12	300	25	— ≥ 31
C	Freq-R	3.95-5.85	5.75-6.75	4.5-5.1	6.0-7.0
	SEFD	10	25	61	80 28
X	Freq-R	8.00-10.1	7.9-9.0	8.1-8.7	—
	SEFD	15	18	170	— ≥ 38

Table 1: 国际上进行脉冲星观测研究的同类型大型望远镜性能参数

2 上海65米射电望远镜脉冲星试观测结果

2013年1月，上海65米射电望远镜进行了脉冲星试观测。观测终端为脉冲星数字化滤波阵列(PDFB)，观测波段为S和X，观测带宽分别为~150 MHz和~350MHz。本次试观测选取了各类脉冲星进行广泛测试。图1展示了正常脉冲星J2022+2854，毫秒脉冲星J2145-0750 (P=16 ms)，高色散量脉冲星J0248+6021 (DM=370 cm⁻³pc)

的S波段观测结果以及B0355+54的X波段观测结果。这四颗脉冲星在1.4 GHz的流量密度分别是38 mJy, 8.9 mJy, 13.7 mJy和23 mJy。此次观测积分时间分别是3 min, 18 min, 15 min和5 min。从图1中可以看出, 尽管在S和X波段存在一些干扰, 但是这些干扰在可控范围之内。上海65米射电望远镜高频波段脉冲星观测能力也“可见一斑”, 对于在1.4 GHz流量密度为23 mJy的脉冲星B0355+54, 该望远镜在X波段仅用5 min观测就可获得非常高信噪比积分轮廓。

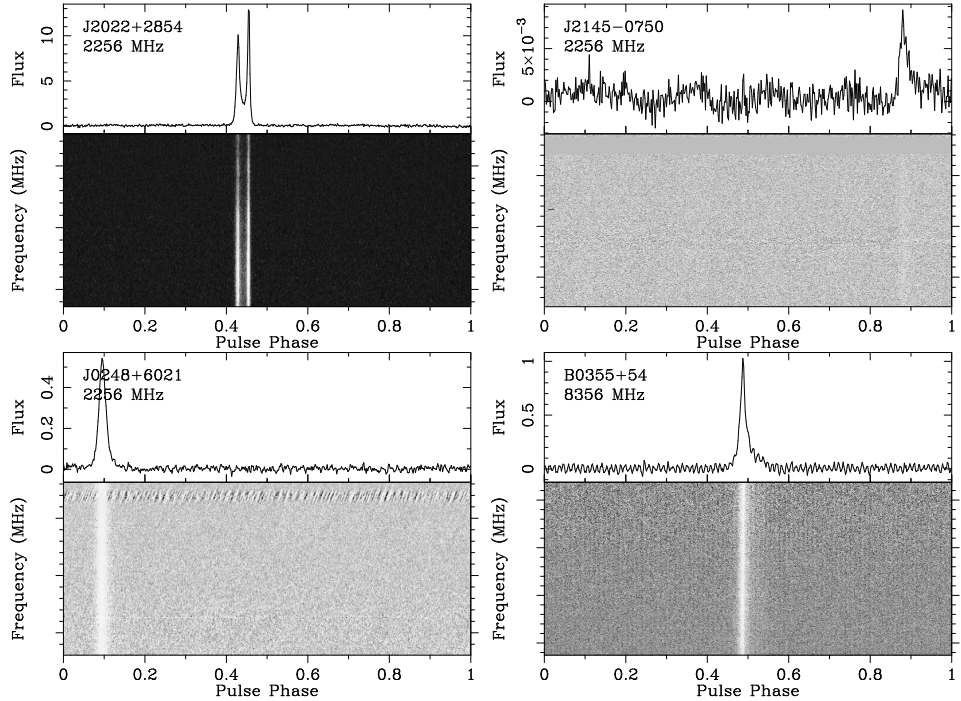


Figure 1: 上海65米射电望远镜脉冲星试观测结果

3 上海65米射电望远镜脉冲星观测研究展望

2013年10月份, 上海65米射电望远镜将配备既有相干消色散功能又有非相干消色散功能的脉冲星数字化终端(DIBAS)。相干消色散模式, DIBAS可支持的最大带宽为800 MHz。非相干消色散模式, DIBAS可支持的最大带宽为6000 MHz。该系统既支持搜寻模式的脉冲星观测又支持在线叠加模式的脉冲星观测。利用该系统, 上海65米射电望远镜将有计划地开展如下方向的脉冲星观测研究:

(一) 脉冲星搜寻:为克服上海65米射电望远镜目前无多波束接收机系统, 我们计划在银心附近、球状星团、无对应体的 γ 射线源等一些高发现概率区域进行有的放矢的脉冲星搜寻。搜寻将在C波段进行。尽管脉冲星流量会随频率升高而降低, 但C波段的脉冲星搜寻和其它低频波段相比具有一定的自身优势: (1) 对于银心

周围的脉冲星，只有高频辐射才能穿过该区域浓密的等离子体；（2）更低的银河系背景噪声；（3）更弱的星际闪烁、色散以及散射效应等。

（二）脉冲星多波段积分轮廓以及流量密度测量：脉冲星多波段积分轮廓以及流量密度测量对进一步揭示其辐射机制具有重要意义。目前，绝大多数脉冲星具有在400 MHz和（或）1400 MHz的积分轮廓以及流量测量结果，但仅有极少数脉冲星具有高频(>3 GHz)积分轮廓及流量密度测量结果[6]。为此，我们将发挥上海65米射电望远镜高频（尤其是C波段）优势，近期将测定PSR B0950+08等60颗强脉冲星C波段积分轮廓和流量密度。对于部分强脉冲星，测量会扩展到X波段。

（三）单脉冲模式下脉冲星以及脉冲星类天体的观测研究：单脉冲模式的观测对于研究巨脉冲以及射电暂现源（RRAT）的辐射机制具有重要意义[7]。我们计划在L波段对巨脉冲现象脉冲星以及RRAT进行监测以进一步揭示其辐射机制。

（四）脉冲星模式变换以及零脉冲现象观测研究：研究表明脉冲星的模式变换和零脉冲现象之间具有一定的相关性[8]。为进一步研究模式变换和零脉冲现象，揭示二者之间的相关性，上海65米射电望远镜将对脉冲星B0809+74等进行监测。

（五）银心周围脉冲星监测：受银心周围浓密等离子的影响，目前仅有几颗脉冲星被发现，如J1746-2850I以及磁星J1745-2900等。银心附近的脉冲星的监测，不仅可以揭示脉冲星自身物理，而且可以揭示银心的物理环境。我们计划发挥上海65米射电望远镜在C波段的优势，对这些脉冲星进行长期监测。

（六）脉冲星到达时间观测：上海65米射电望远镜将对部分特殊脉冲星进行到达时间监测，如具有周期跃变现象的脉冲星，引力波探测阵列毫秒脉冲星等。

此外，上海65米射电望远镜还为国内外科研人员提供观测服务。总之，我们将充分发挥上海65米射电望远镜系统的优势，开展一系列脉冲星以及脉冲星类天体的观测研究工作。

*本研究是上海65米射电望远镜项目组集体智慧的结晶。感谢国家天文台、云南天文台借用PDFB；感谢郝龙飞、李志玄，岳友岭，刘志勇等在PDFB使用方面给予帮助。本项研究工作得到了上海市科学委员会的资助，资助课题编号为:08DZ1160100和13ZR1464500。

References

- [1] Lorimer D. R. and Kramer M. . Handbook of Pulsar Astronomy. December 2004.
- [2] Han, J. L. 2008, Nuclear Physics B Proceedings Supplements, 175, 62
- [3] <http://www.gb.nrao.edu/fghigo/gbtdoc/vlbinfo.html>
- [4] http://www.evlbi.org/user_guide/EVNstatus.txt
- [5] http://www.parkes.atnf.csiro.au/observing/documentation/user_guide/
- [6] <http://www.atnf.csiro.au/research/pulsar/psrcat/>
- [7] Esamdin, A., Abdurixit, D., Manchester, R. N., & Niu, H. B. 2012, ApJ, 759, L3
- [8] Wang, N., Manchester, R. N., & Johnston, S. 2007, MNRAS, 377, 1383

Re-processing the Parkes Multi-beam Pulsar Survey Data: Software test and initial result

Meng Yu

*National Astronomical Observatories of China
20A Datun Road, Chaoyang District, Beijing 100012
P. R. China
E-mail:vela.yumeng@gmail.com*

Re-processing the Parkes Multi-beam Pulsar Survey (hereafter PM) data at the NAOC FAST project group was started in March 2013. The goal of this work is to study the pipelines on searching for isolated pulsars, pulsars in binary systems and single-pulse/radio-burst events with developing relevant routines for various pulsar-related researches; these appear to be a preparation for the future FAST pulsar survey programme. The available PM survey data set comprises 50,399 PSRFITS data files (100MB per file). Fig. 1 shows the positions (in J2000 Geocentric Coordinate System) of all the pointings covered by the PM survey. Up-till-now, more than 26,070 ($\sim 52\%$ of the total) data files have been processed and 20,125 candidates from 1,282 data files ($\sim 2.5\%$) have been reviewed. Among the reviewed candidates, we confirm the detection of six known pulsars.

We used the searching software package PRESTO¹ to process the data. The whole routine is running on a computing cluster that includes five nodes with containing 64 CPU cores. The current pipeline aims at searching for isolated pulsars with analysing their single pulses; it includes (routines used are indicated in parentheses):

- RFI removal (`rfifind`)
- “Tree” algorithm de-dispersion (`prepsubband`)
- FFT and periodicity search (`realfft` and `accelsearch`)
- Folding for obtaining the candidates (`prepfold`)
- PICS (Pulsar Image-based Classification System) candidate ranking[1]
- Search for pulsar single pulses (`single_pulse_search.py`)

The current pipeline did not include any binary searching routine. Searching for binaries will be carried out in the next step. As an example, in Fig. 2, we show the diagnostic plot for the detection of PSR J1141–6545. Table 1 summarises the pulsar parameters of the detected six pulsars.

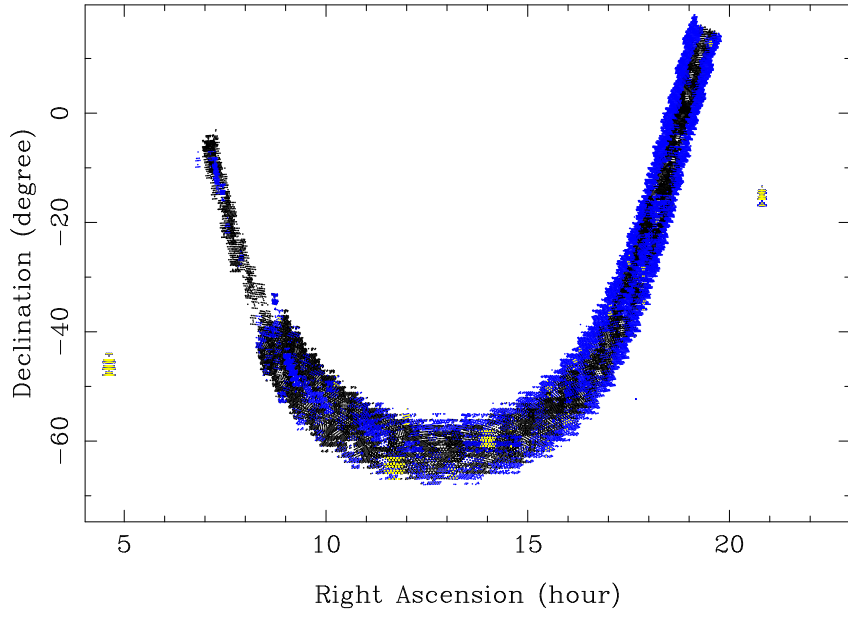


Figure 1: Positions (J2000) of all the pointings covered by the PM survey. The blue points indicate the data that have been processed, while the yellow points indicate the data from which the candidates have been reviewed.

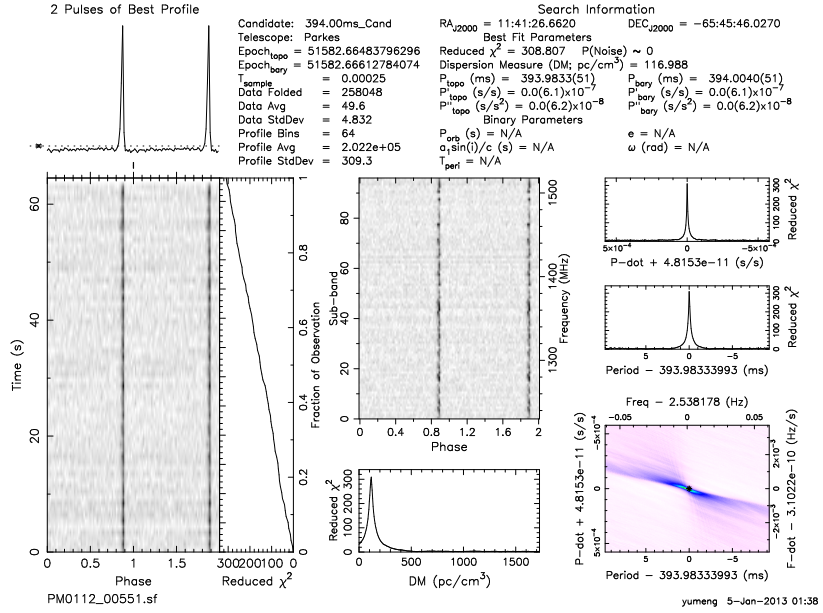


Figure 2: Diagnostic plot for the detection of pulsar J1141–6545.

Table 1: Positions, periods and DMs of the detected six known pulsars.

PSR J	R.A. (J2000) (h:m:s)	Dec. (J2000) (° ' '')	P (s)	Epoch (MJD)	DM (cm ⁻³ pc)
J0437–4715	04:37:15.6967	–47:15:08.0520	5.7578609(14)	51561.4	2.562
J1141–6545	11:41:26.6620	–65:45:46.0270	393.983(6)	51582.7	116.988
J1359–6038	13:59:59.8303	–60:38:06.9750	127.5040(4)	51692.4	294.188
J1435–5954	14:35:00.3050	–59:54:48.0000	473.02(9)	51635.5	45.402
J1701–3726	17:00:53.4554	–37:33:16.3680	2452.689(5)	51718.6	308.434
J1933+1304	19:33:03.9458	+13:08:34.0680	928.271(4)	51693.8	169.625

MY thanks Dr. R. N. Manchester and Dr. G. Hobbs for their approval and great efforts for copying the whole data set of the PM survey. MY also thanks the kind help from many colleagues, including Dr. Di Li, Dr. Youling Yue, Dr. Xinping Deng and Mr. Jiguang Lu.

References

- [1] Zhu W. W. et al., 2013, arXiv:1309.0776

¹<http://www.cv.nrao.edu/sransom/presto/>

Magnetar Giant Flares and Precursors

Cong Yu

Yunnan Observatories

Chinese Academy of Sciences

Yunnan 650011

P. R. China

Email: cyu@ynao.ac.cn

1 Introduction

Two closely related types of high-energy sources – Anomalous X-ray Pulsars (AXPs) and Soft Gamma-ray Repeaters (SGRs), are well explained as magnetars, neutron stars with super-strong ($10^{14} - 10^{15}$ G) magnetic fields. It is commonly accepted that dissipation of the magnetic fields drives persistent and bursting emission [1].

Precursors to giant flares have been identified. For instance, the 2004 giant flare was proceeded by a 1 second long energetic outburst event. The energy from the precursor is estimated to be about 10^{42-43} ergs. After the precursor, the magnetar entered a temporary quiescent state and stayed in the quiescent state for about 140 seconds. Then it finally gave rise to the more violent flare. It is inferred that the precursor and the giant flare are causally related. This precursor is hard to explain by our previous model, since the catastrophic state transition could take place only once due to the single critical point appearing in the equilibrium curve. Additional physical elements should be included [2].

It is conceivable that, once the flux rope loses its equilibrium, a current sheet can be generated in the magnetosphere. This type of current sheet provides an ideal place for magnetic reconnection.

2 Magnetosphere with current sheets and flux rope

We show the schematic diagram of our model in the left panel of Fig. 1. The toroidal force-free magnetic flux rope, shown by a thick dashed circle, is suspended by force balance in the magnetosphere at the height, h , measured from the neutron star center. In the interior of the helically twisted flux rope, the Lundquist solution is used. A simple relation between r_0 (minor radius of the rope) and I (current carried by the rope), i.e., $r_0 = (r_{00}I_0)/I = r_{00}/J$, is valid for such flux ropes. The quantity I_0 is related to the magnetar radius r_s and a constant Ψ_0 (with magnetic flux dimension)

by $I_0 = (\Psi_0 c)/r_s$. Here c stands for the speed of light. The dimensionless current $J = I/I_0$ is the current measured in unit of I_0 . The parameter r_{00} is fixed as 0.01, which is the value of r_0 for $J = 1$. For convenience of numerical calculations, lengths are measured in r_s , magnetar radius. Currents are measured in I_0 and the magnetic fluxes in Ψ_0 .

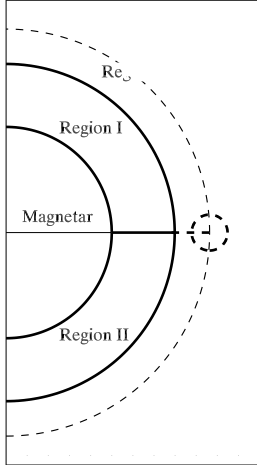


Figure 1: Magnetosphere containing a twisted flux rope and a current sheet. *Left:* The radius of magnetar is denoted by r_s . The current sheet is designated as the thick horizontal line at the equator, the height of which is denoted by r_1 . The twisted flux rope is designated as thick dashed circle at the equator, the height of which is denoted by h . The computation domain is divided into three regions. Solutions in different regions are obtained separately and finally melted together to form a global solution. *Right:* The magnetic field lines (thin solid line) and the current sheet (thick solid line) are shown.

In our model, the twisted flux rope would lose its equilibrium due to the quasi-static evolutions at the surface and finally erupt abruptly. We find that there may exist two critical points in the flux rope equilibrium curve when current sheets are taken into account. According to this new feature, the precursor and the giant flares can be naturally explained as two stages in the evolution of our models. The dynamical state transitions around the two critical points correspond to the precursor and the giant flares, respectively. The stable branch between the two transitions represents the quiescent state between the precursor and the giant flare.

3 Conclusion

We focus on the possibility of magnetospheric origin for the precursors and the successive giant flares. We put forward a force-free magnetosphere model containing a helical flux rope and a current sheet below the flux rope. The catastrophic response of the flux rope is examined in detail, taking into account the gradual process of flux injections at the ultra-strongly magnetized neutron star surface. The detailed energetics of the model are also discussed. The magnetic energy release fraction in the first jump is consistent with the precursor energy budget. The energy release fraction in the second jump, which corresponds to the giant flare is lower than the value inferred from observations. This shows that additional energy release is necessary to account for the giant flare. The current sheet generated by the catastrophic loss of equilibrium behavior of the flux rope also provides an ideal place for magnetic reconnection, which can further enhance the energy release during the eruptions. How magnetic reconnection affects the energy release needs further investigations.

References

- [1] Duncan, R. C., & Thompson, C., ApJL, **392**, 9 (1992)
- [2] Yu C. & Huang L., ApJL, **771**, 46 (2013)

脉冲星的到达时间观测

袁建平, 李琳, 刘志勇, 王娜, 王晶波, 朱翠
中国科学院新疆天文台
中国 新疆 乌鲁木齐830011
Email: yuanjp@xao.ac.cn

1 引言

对射电脉冲星的脉冲到达时间 (Time of Arrival, TOA) 进行常规的监测, 可以用来研究脉冲星的自转与双星轨道运动, 也可以用来探测星际介质, 甚至可以用来探测引力波。对脉冲星进行多波段的到达时间观测, 还可以用来测量色散量 (DM) 的变化, 这有助于修正脉冲轮廓, 从而获得准确的高精度的到达时间。

2 观测和结果

帕克斯多波束巡天发现了800多颗脉冲星[9], 其后的巡天有阿雷西博L波段馈源阵巡天[5], 高时间分辨率宇宙巡天[8], 英仙臂巡天[2]。其发现的脉冲星有一部分的流量密度超过了南山25米射电望远镜的灵敏度 (0.5 mJy)。我们使用南山25米射电望远镜对新发现的较强脉冲星进了观测。观测的中心频率是1540 MHz, 带宽320 MHz。终端采用多通道数字滤波器组 (Digital Filter Bank) 来记录中频信号。每颗星观测的时长为12 – 16 分钟, 数据处理采用标准的到达时间数据处理方法, 数据处理软件使用PSRCHIVE 和TEMPO2。

表格1 列出了九颗脉冲星的观测结果 (我们只拟合了自转频率的变化率)。PSR J0627+0706 是加州理工-阿雷西博巡天发现的[4], 特征年龄为2.5 万年, 是年轻的脉冲星。从它被发现到现在已经十年了, 目前还没有探测到周期跃变。在未来几年或十几年内, 它可能发生周期跃变, 有必要继续对它进行到达时间观测。PSR J1730–2304 是毫秒脉冲星, 由于南山的模拟消色散系统的时间分辨率不高, 不能观测周期为几毫秒的脉冲星 (能观测周期是十几毫秒的源)。2010 年1 月投入使用的数字消色散系统采用高时间分辨率采样, 能观测九颗毫秒脉冲星。PSR J1828–0611、J1823–0823 和J1843–0000 是2004年才报道的帕克斯巡天发现的脉冲星[7]。PSR J1844+00 在1996年就发现了[3], 但是只报道了周期频率, 没有报道自转减慢率, 英国洛韦尔76米射电望远镜探测到它的两次周期跃变[6]。南山25 米射电望远镜测得它的自转减慢率 $\dot{P} = 1.6682(4) \times 10^{-15} \text{ s s}^{-1}$, 那么它自转能损率是 $6.7 \times 10^{32} \text{ erg s}^{-1}$, 特征年龄是 4.37×10^6 年, 表面磁场是 8.87×10^{11} 高斯。可以看出PSR J1844+00 是一颗非常普通的脉冲星, 没有什么特别之处。

Table 1: 脉冲星的自转参数。第一列是脉冲星的名字，第二、三列是南山25米射电望远镜测得的自转频率和自转频率变化率。第四、五列是自转频率的历元和数据跨度，最后两列是TOA的个数和到达时间残差。

Name PSR J	ν (Hz)	$\dot{\nu}$ (10^{-15} s^{-2})	Epoch (MJD)	Data span (MJD)	Number of TOAs	Residual (μs)
0627+0649	2.885812601174(9)	-14.087(3)	56415	56294 – 56536	8	26
0627+0706	2.1013619189117(12)	-131.59(6)	56404	56294 – 56515	6	382
0646+0905	1.106300834925(15)	-1.112(17)	56384	56294 – 56474	8	190
1730–2304	123.11028902078(11)	-0.09(2)	56343	56151 – 56536	17	14
1828–0611	3.711742299165(20)	-20.069(6)	56199	55862 – 56536	16	348
1831–0823	1.633631675364(6)	-0.84158(17)	56294	56053 – 56536	11	82
1843–0000	1.135933215133(16)	-10.083(4)	56318	56101 – 56536	11	268
1844+00	2.171534216035(18)	-7.8667(16)	56051	55586 – 56516	44	622
2027+4557	0.909379097406(7)	-0.2558(8)	56189	55863 – 56516	35	322

3 讨论

脉冲星具有地面实验室不能到达的极端物理环境，脉冲星自转的不稳定性（比如周期跃变）被认为是中子星内核致密超流的物理变化引起的，因此，对自转不稳定性的研究有助于我们理解中子星的内部结构和自转演化。脉冲星周期跃变也可能会触发中子星表面加热或者磁场的再结合（这两种物理过程可能与X射线和伽玛射线辐射有关[11, 10]）。周期跃变还可能是中子星发生形变（比如椭率发生变化）引起的，从而激发引力波[1]。为了多波段设备能及时的跟进观测，需要迅速准确探测到周期跃变发生的时间，这只有通过常规的到达时间观测。而且，研究费米卫星和其他望远镜（比如MAGIC）探测到的脉冲星的高能辐射，需要射电望远镜提供精准的脉冲星自转参数。

前几年发现的几类具有射电辐射的中子星：旋转射电暂现源（RRAT）、间歇脉冲星和射电噪磁星，拓展了我们对中子星的认识。到达时间观测研究表明他们具有与普通脉冲星类似的性质，比如自转周期和自转减慢与普通脉冲星一致。他们也有与普通脉冲星不一致的特性。它们的射电辐射不是持续的，而是间歇爆发的，极端情况下甚至一天时间里只有一秒的时间在爆发辐射。对它们进行到达时间观测可以测量它们的基本参数，比如自转周期和周期减慢率，这样可以更好的认识这些脉冲的特征，从而有助于我们理解RRAT、间隙脉冲星以及磁星与普通脉冲星的关系。

致谢

本工作受国家重点基础研究发展计划（2012CB821800）和中国科学院“西部之光”基金（XBBS201021）支持。

References

- [1] Bennett, M. F., van Eysden, C. A., & Melatos, A. 2010, MNRAS, 1370
- [2] Burgay, M.; Keith, M. J.; Lorimer, D. R.; et al.; 2013, MNRAS, 429, 579
- [3] Camilo, F., Nice, D. J., Shrauner, J. A., et al., 1996, 469, 819
- [4] Chandler, A. M., 2003. PhD thesis, California Institute of Technology.
- [5] Cordes, J. M.; Freire, P. C. C.; Lorimer, D. R. et al.; 2006, ApJ, 637, 446
- [6] Espinoza, C. M., Lyne, A. G., Stappers, B. W. et al. 2011, MNRAS 414, 1679
- [7] Hobbs, G., Faulkner, A., Stairs, I. H., et al., 2004, MNRAS, 352, 1439
- [8] Keith, M. J.; Jameson, A.; van Straten, W.; et al.; 2010, MNRAS, 409, 619
- [9] Manchester, R. N.; Lyne, A. G.; Camilo, F.; et al.; 2001, MNRAS, 328, 17
- [10] Tang, A. P. S., & Cheng, K. S. 2001, ApJ, 549, 1039
- [11] Van Riper, K. A., Epstein, R. I., & Miller, G. S. 1991, ApJ, 381, L17

40米望远镜脉冲星搜索终端

岳友岭 朱岩
中国科学院国家天文台
中国北京100012
Email: [yueyouling\(at\)gmail.com](mailto:yueyouling(at)gmail.com)

1 引言

随着天文学研究越来越向探测微弱信号的方向发展，天文仪器的灵敏度也不断提升。射电天文的终端技术紧随工业技术发展，但是直至本世纪初，终端的开发速度还较缓慢，一台终端的研制需要一年至几年的时间。由于数字采样技术和可编程门阵列（FPGA）技术的进步，射电天文数字终端在最近10年有了飞速发展，开发周期逐步缩短。

加州大学伯克利分校的 CASPER (Collaboration for Astronomy Signal Processing and Electronics Research) 实验室^[1] 开发的模拟数字转换器 (ADC) 和 ROACH (Reconfigurable Open Architecture Computing Hardware) 系列可编程数字处理板卡是这方面的典型应用。CASPER的硬件都是开源设计，同时提供了大量的开源软件和丰富的文档。对于有使用经验的开发者，可在2至3个月内使用这套硬件平台开发一套新的终端。

本文介绍了使用ROACH数字板卡和配套ADC，为云南天文台40米射电望远镜研制的一套脉冲星数字终端。该终端实现了脉冲星搜索功能，试观测结果良好。

2 40米望远镜脉冲星搜索终端

该终端由使用iADC和ROACH硬件平台，同时配以x64服务器用于控制和数据接收存储。ROACH与服务器采用10GbE网络连接，4路10GbE的整体数据传输速度可接近4GB/s。实际的数据存储速度受限于服务器硬盘。观测固件基于Parkes望远镜脉冲星终端的Parspec^[2]。该固件最初基于IBOB平台，后被移植到RAOCH平台。我们做了一些修改使其适于我们脉冲星搜索观测应用，并开发了数据接收程序及观测界面。该终端主要指标如下：

- 1024M 采样/s, 8 bits, 512MHz 带宽
- 1024 通道
- 2 偏振
- 最高时间分辨率: 4微妙
- 数据格式: PSRFITS

观测界面由三部分组成: 控制、显示、数据接收, 各为一个进程运行。控制和显示界面由Python开发, 便于调试和更新, 接收程序由C开发。

3 试观测及科学目标讨论

2013年6月底在云南天文台40米望远镜进行了试观测, 观测到了B0329+54等多颗脉冲星, 效果良好。同时观测到了vela脉冲星的单个脉冲, 表明终端具备高时间分辨率观测的能力。建议重复新疆天文台一些工作以进行对比, 测试系统性能并积累观测经验。利用该终端可开展巨脉冲、单个脉冲、RRAT、模式变换及消零(nulling) 等观测研究。待积累了一些观测经验后可开展单个射电暴发的巡天, 积累观测数据处理经验。有了这些实际的观测和数据处理经验, 可迅速投入FAST巡天数据的处理。

终端的使用、调试及数据等信息将逐步添加到 <http://pulsar.bao.ac.cn/wiki/>。

致谢

本项目的开发和试观测得到云南天文台、国家天文台和北京大学的大力支持。项目由国家重点基础研究发展计划(2012CB821800)和国家自然科学基金(11103045)资助。

参考文献

- [1] <https://casper.berkeley.edu/>
- [2] <https://casper.berkeley.edu/wiki/Parspec>

脉冲星周期跃变中的能量释放

周恩平 (*Enping Zhou*)
北京大学物理学院天文学系
中国 北京 100871
Email: zhouenpingz715@sina.com

1 引言：脉冲星的周期跃变

转动供能的脉冲星在辐射过程中损失自转能从而会自转减慢，然而对于许多转动供能的脉冲星，其自转除了会随着时间变慢之外，还会在特定时间发生周期变短的跃变。在不同的脉冲星物态模型中，这种周期跃变现象也都有其对应的理论模型。

在中子星模型中，星体的不同壳层之间存在着较差转动，我们观测到的脉冲周期其实是外壳层的转动周期，而在一定情况下，内外壳层会通过超流中子涡丝的钉扎效应 (pin) 发生耦合，形成共转，从而旋转较快的内层会“拉”动较慢的外层，形成我们所看到的周期跃变现象。

而在固态夸克星模型中，一般认为周期跃变现象的发生是由于星体发生了星震，形变使得星体的转动惯量发生了改变（通常是减小），在角动量守恒的情况下，便会使脉冲星的周期发生变短的跃变。

然而值得注意的是，脉冲星的周期跃变过程中，伴随着的能量释放的特征，则是不尽相同的，一种是像Vela这样的脉冲星，虽然经常发生大的周期跃变，周期跃变时在各个波段的观测数据中却没有看到很明显的流量增加，另一种是像AXP/SGR这样的脉冲星，在发生周期跃变的同时往往伴随着高能波段的流量增加。

无论是哪种理论模型，如果想要顺利成章得解释脉冲星周期跃变现象，那它必须也能在一个框架下解释这两种在能量释放上截然不同的周期跃变现象。而我所要讨论的内容，就是如何在固态夸克星的模型下，去理解这两种周期跃变现象。

2 固态夸克星模型下的两种周期跃变现象

对于自束缚的小质量的固态夸克星，由于与中子星的引力束缚不同，其质量半径关系也与中子星明显不同，其质量近似于半径的三次方增长，而当质量增大到一个太阳质量左右时，引力的束缚已经变得不可忽略，因而其质量半径关系会表现出与中子星类似的趋势，半径会随着质量的变大而变小，这也就使得夸克星存在一个最大半径，而这一最大半径对于理解AXP/SGR这样的伴随着能量释放的周期跃变是很有趣的。

许多证据表明，AXP/SGR通过周围的回落盘进行着吸积，如果其半径本身已经接近最大半径，那么在吸积物质质量增大的过程中，星体最稳定状态的半径反而会减小。但是由于固体的刚性，星体的半径并不可能完全随着质量半径关系给出的稳定半径演化，在这种情形下，星体的半径超过最稳定状态的理论半径，会积累大量的弹性能。随着吸积的进行，此偏离越来越大，弹性能积累也越来越多，当超过固体的应力极限时，星体会发生破碎，整个星体的半径变小。对于这一类的周期跃变现象，通过定量计算可以知道，对于转动和引力平衡的刚体，其引力能释放与转动能增加刚好相等，故不会有能量放出，而当转动慢于此平衡转速时，转动能的增加与引力能的减小量之间的差距迅速增大。由于绝大多数AXP/SGR的自转都很慢，自转周期远大于转动和引力平衡的周期0.7ms，故在周期跃变过程中，转动能的增加与引力能的释放相比几乎可以忽略，故在这类周期跃变中，会有大量的能量最终于辐射的形式爆发出来，能量的多少取决于周期跃变的幅度。

另一种情形则与星体的冷却和自转减慢有关。一般认为，一个旋转的流体星球，其平衡位形应该是一个马克洛林椭球。而铁核塌缩过程形成的原初脉冲星，在诞生初期温度很高，可以认为是流体，在其损失转动能自转变慢的过程中，其平衡位形按照马克洛林椭球给出的位形变化。当脉冲星冷却到一定温度时，星体会发生固化，之后星体的位形就不能完全按照马克洛林椭球给出的椭率发生变化，椭率大于理论上的平衡位形的椭率，开始积累弹性能。随着星体损失转动能自转变慢，星体实际位形与马克洛林椭球给出的位形偏差也会变大，当弹性能积累到一定程度时，星体会发生破碎，椭率会突然变小，发生周期跃变现象。由于星体整体位形变化并不多，引力能的释放并不多，而考虑星体的平衡位形条件，可以定量得计算出在这类周期跃变现象中弹性能、引力能的减少量与转动能的增加量之间的关系，计算结果表明，即使对于Vela脉冲星发出的一些较大的周期跃变，也可以几乎不放出能量。

定性上来理解，造成这种差别的主要原因在于，赤道附近的物质，对于转动惯量有着最大的贡献，而极区的物质，虽然和赤道附近的物质一样贡献着引力能，但是对转动惯量却几乎没有贡献，因此在整个星体发生塌缩的第一种图像里，有许多物质释放了引力能，但是却并没有引起转动惯量的明显变小，因而转动能增加并不明显，而在第二种图像里，星震过程中星体体积保持不变，只是椭率改变，近似得可以看做把赤道区域的一部分物质转移到了极区，引力能并没有发生明显的变化，但是转动惯量却变化明显，因而损失的能量基本全部转化为转动能，而没有多余的能量通过辐射来释放。

3 总结

在固态夸克星框架下，我们可以通过有吸积、体积变化的星震和体积不发生变化的星震这两种模型，来理解观测中有能量释放和没有能量释放的两种脉冲星周期跃变现象。

Scientific Program of FAST Pulsar Symposium 2

July 1-3, 2013, Kunming, China

(Language: **English or Chinese**; but the presentation should be written in English)

===== Monday, July 1 =====

8:30 -- 11:30 Registration (Dian Chi Hotel, Kunming)

Conference Opening

Chair: Renxin Xu (30min = 25+5)

14:00 -- 14:10: Welcome addresses by Dr. Jiancheng Wang

14:10 -- 14:20: LOC message by Dr. Min Wang

14:20 -- 14:50 Fredrick Jenet: *Pulsars, Radio Transients, the center for advanced radio astronomy, and FAST*

14:50 -- 15:20 Andrew Siemion: *The CASPER approach to open-source radio astronomy instrument design*

15:20 -- 16:00 *Taking a photograph, Coffee Break*

Session 1: Pulsar observations I

Chair: Min Wang (20min = 15+5)

16:00 -- 16:20 Guojun Qiao: *To test pulsar radiation models by Chinese telescopes*

16:20 -- 16:40 Lin Li: *Positions and proper motions for 20 pulsars*

16:40 -- 17:00 Meng Yu: *Re-processing for the archival Parkes survey data*

17:00 -- 17:20 Youling Yue: *A pulsar backend for YNAO telescope based on CASPER hardware*

17:20 -- 17:40 Jintao Luo: *Accelerate pulsar searching with GPU*

18:00 -- 20:00 Banquet

===== Tuesday, July 2 =====

Session 2: Pulsar observations II

Chair: Hongguang Wang (20min = 15+5)

08:00 -- 08:20 Andrew Siemion: *Exploring the Galactic center neutron star population*

08:20 -- 08:40 Biping Gong: *On the timing behavior of 4U 1627-67*

08:40 -- 09:00 Zhigang Wen (J. Yuan): *Detection of strong pulses from PSR J1239 at 1540 MHz*

09:00 -- 09:20 Zhixuan Li: *Coherent de-dispersion pulsar backend project at YNAO*

09:20 -- 10:00 *Coffee Break*

Session 3: Pulsar astronomy and astrophysics I

Chair: Longfei Hao (20min = 15+5)

10:00 -- 10:20 Hongguang Wang: *New insight to the radio emission beam of pulsars*

10:20 -- 10:40 Jianping Yuan: *Pulse nulling of three pulsars*

10:40 -- 11:00 Yuanjie Du: *Multi-wavelength pulsed emission from millisecond pulsars*

11:00 -- 11:20 Zhiqiang Yan (B. Gong): *Precession induced slow glitches on pulsar B1822-09?*

11:20 -- 11:40 Zhibing Li: *Energy dependence of LF QPOs for BH H1743-322 and NS Cyg X-2*

Session 4: Pulsar astronomy and astrophysics II

Chair: Jianping Yuan (20min = 15+5)

14:00 -- 14:20 Zhaosheng Li: *The accretion rate independence of horizontal branch oscillation*

14:20 -- 14:40 Zhibing Li: *Alfven wave model for correlations between kHz QPO and LF QPOs*

14:40 -- 15:00 Guo-Jie Cao: *The effect of differential rotation on the magnetic field*

15:00 -- 15:20 Zhifu Gao: *Constraining braking indexes of magnetars by supernova remnants*

15:20 -- 16:00 *Coffee Break*

Session 5: Pulsar astronomy and astrophysics III

Chair: Biping Gong (20min = 15+5)

16:00 -- 16:20 Weiwei Zhu: *Testing gravity theories with high-precision pulsar timing*

16:20 -- 16:40 Dehua Wang: *The constrain of NS Mass-Radius by kHz QPOs*

16:40 -- 17:00 Shi Dai: *Pulsar mass measurements with gravitational microlensing*

17:00 -- 17:20 Jiguang Lu: *To differentiate neutron star models by X-ray polarimetry*

17:20 -- 17:40 Liang Dong: *Under sampling technology: a new design idea for radio terminals*

===== Wednesday, July 3 =====

Session 6: Magnetars

Chair: Youling Yue (20min = 15+5)

08:00 -- 08:20 Hao Tong: *Low magnetic field magnetars*

08:20 -- 08:40 Cong Yu: *Magnetar giant flares and their precursors*

08:40 -- 09:00 Yanjun Guo: *X-ray spectra of magnetars*

09:00 -- 09:20 Wei Wang: *Understanding accreting and isolated magnetars in hard X-rays*

09:20 -- 09:40 Xiongwei Liu: *Braking pulsars by fossil disk: from radio pulsar to magnetar*

09:40 -- 10:20 *Coffee Break*

Session 7: Free Discussions

Chair: Renxin Xu

10:20 -- 10:40 Zhen Yan: *Pulsar Science with Shanghai 65m Radio Telescope*

10:40 -- 12:00 *Discussions: science, cooperation and others*